Coupled Plasmonic Nanowires: Dual-Channel Fourier Microscopy Studies

A thesis

submitted in partial fulfilment of the requirements
for the degree of Doctor of Philosophy

by

Danveer Singh
(Reg ID: 20123220)

INDIAN INSTITUTE OF SCIENCE EDUCATION AND RESEARCH
(IISER), PUNE

CERTIFICATE

Certified that the work incorporated in the thesis entitled ("Coupled Plasmonic Nanowires: Dual-channel Fourier Microscopy Studies") Submitted by **Danveer Singh** was carried out by the candidate, under my supervision. The work presented here or any part of it has not been included in any other thesis submitted previously for the award of any degree or diploma from any other University or institution.

Date: (Supervisor)

Declaration

I declare that this written submission represents my research work in my own words and where others' ideas or works have been included, I have adequately cited and referenced the original sources. I also declare that I have adhered to all principles of academic honesty and integrity and have not misrepresented or fabricated or falsified any idea/data/fact/source in my submission. I understand that violation of the above will be cause for disciplinary action by the Institute and can also evoke penal action from the sources which have thus not been properly cited or from whom proper permission has not been taken when needed.

Date: (Signature)

Danveer Singh

Reg. No: 20123220

Abstract

Transmission and localization of light at subwavelength scale has direct relevance in the nanophotonic-circuits of light. Usage of dielectric materials hampers nanophotonic operations due to diffraction limit of light. To overcome this problem, plasmonic nanostructures made of metals such as silver and gold have been utilized. They show unique optical properties at subwavelength scales, such as enhanced localization of electric fields, sub-diffraction limit light propagation, directional emission and optical antenna effects, which can be harnessed in chip-scale integrated photonics and optoelectronics. This has motivated research in identifying novel optical nanostructures that can efficiently perform optical operations at sub-wavelength scale. With this hindsight, we have experimentally developed and studied unique nanophotonic architecture: serially-coupled plasmonic nanowires, and observed the capability of light transmission and polarized emission beyond diffraction limit of light. In order to control the light transmission and emission, the geometry of coupled nanowire system were optimized. The optimization parameters were bending angle between nanowires, excitation profile and coupling geometry. Upon optimization, we tested the capability of routing the light as a function of polarization of incident light and showcased the ability of polarization beam splitting at sub-wavelength scale. In order to further understand the light emission characteristics from such nanowire systems, it was important to develop advanced optical microscopy methods to probe angular scattering and emission characteristics. To fulfill this requirement, we have designed and developed an advanced dual-channel Fourier optical microscopy and spectroscopy system to study the directional optical emission from individual plasmonic nanowires and nanoparticle-nanowire system. An important aspect of our microscope is the measurement of k-vector distribution of light emanating from an individual, supported nanowire through the substrate and superstrate. I have explained how our home-built optical microscope can probe far-field directional emission properties of an individual nanowire and nanoparticle-coupled nanowire architectures resting on a dielectric substrate. I have emphasized upon the ability to capture optical images in Fourier-plane and spectroscopic signatures in real-plane through a substrate and superstrate. Our work pushes the limit of optical characterization of nanoscale structures, and can be utilized to address relevant questions pertaining to interaction of

light with individual nanowires.

List of Publications

Included in thesis:

- Angular Emission from an 1D and 2D meso- and nano-structures: Probed by Dual-Channel Fourier-Plane Photoluminescence Microscopy; **Danveer Singh**, Deepak K Sharma, Shailendra Kumar Chaube, G V Pavan Kumar. *Optics Communications, 398, 112-121 (2017)*

- Directional Out-Coupling of light from Plasmonic Nanowire-Nanoparticle Junction ; **Danveer Singh**, Arindam Dasgupta, Aswathy V.G., Ravi P.N. Tripathi, G. V. Pavan Kumar, *Optics Letters*, 40, 1006-1009 (2015). (Chosen for Virtual Journal for Biomedical Optics Vol. 10, Iss. 4)

- Polarization controlled light emission and routing in end-to-end coupled plasmonic nanowire dimer; **Danveer Singh**, Mohit Raghuwanshi, G V Pavan Kumar, *Applied Physics Letters*, 101, 111111 (2012).

Not included in thesis:

- Directional Fluorescence Emission Mediated by Chemically-Prepared Plasmonic Nanowire Junctions; Arindam Dasgupta, **Danveer Singh**, Ravi P.N.Tripathi, G. V. Pavan Kumar, and G.V. Pavan Kumar, *Journal of Physical Chemistry C*, 120 ,17692-17698 (2016).

- Evanescent field-assisted intensity modulation of surface enhanced Raman scattering from a single plasmonic nanowire; Sruthi Polali[a], **Danveer Singh**[a] G. V. Pavan Kumar, *Journal of Physics D :Applied Physics*, 46, 195107 (2013); **(a: equal contribution)**.

- Plasmon assisted light propagation and Raman scattering hot-spot in end-to-end coupled silver nanowire pairs; Rohit Chikkaraddya[a] **Danveer Singh**[a], G. V. Pavan Kumar. *Applied Physics Letters*, Appl. Phys. Lett. 100, 043108 (2012), **(a: equal contribution)**.

- Remote-Excitation Surface Enhanced Raman Scattering with Counter-Propagating Plasmons: Silver Nanowire-Nanoparticle System, Arindam Dasgupta, **Danveer Singh**, Shreyash Tandon, Ravi P.N. Tripathi, G. V. Pavan Kumar, *Journal of Nanophotonics*, 8(1), 083899 (2014).

- Subwavelength propagation and localization of light using surface plasmons: A brief perspective; G. V. Pavan Kumar, **Danveer Singh**, Partha Pratim Patra and Arindam Dasgupta, *Pramana - Journal of Physics* (invited review article, NLS-21 issue), 82, 59-70 (2014).

- Highly tapered pentagonal bipyramidal Au microcrystals with high index faceted corrugation: Synthesis and optical properties;9. Gangaiah Mettela, B. Radha, **Danveer Singh**, G. V. Pavan Kumar, G. U. Kulkarni, *Scientific Reports (Nature)*, 3, 1793 (2013)

- Dual-Path Remote-Excitation Surface Enhanced Raman Microscopy with Plasmonic Nanowire Dimer; Arindam Dasgupta, **Danveer Singh**, G. V. Pavan Kumar, *Scientific Reports (Nature)*, 103, 151114 (2013).

Acknowledgements

This is the section where I can tell about the efforts which are paid by the people who constantly provide their supports to accomplish research work during my Ph.D. program. I feel lucky by having such peoples who selflessly provide their time and efforts consistently whenever I need their help.

First of all, I would like to thanks my Ph.D. supervisor Dr. G V Pavan Kumar for providing me a platform to learn science. Under his guidance, I have learned science and gained skills which are important steps to become a good researcher. The long hours discussions with him made me enthusiastic and inspired towards research. It was really a great and learning experience for me to be a part of the journey in a lab which evolves as a full-fledged laboratory today. The important thing which I would like to mentioned here is the freedom which I got from him. This freedom made me to think and perform the experiments without any constraints and boundaries. He always encouraged me to do new things which I thought. The journey with him includes a lot of joy and memorable experience.

I would like to thanks my Research and Advisory Committee (RAC) members, Dr. C. V. Dharmadhikari and Dr. Aparna Deshpande for their constant support and guidance. Their feedbacks and insightful suggestions, during the annual meetings, helped me to improve my research works and better understanding.

I would like to express my sincere thanks to my senior lab members, Dr. Arindam Dasgupta and Dr. Partha Pratim Patra for the constant helps with constructive criticism and valuable suggestion during the research works in the lab. Without their help, it could be difficult to work on the research projects. I have learned many things from them. I have enjoyed a lot of discussions during the tea hours. I sincerely thank my current lab members especially Ravi P N Tripathi, Adarsh B Vasista, Deepak Kumar Sharma for their valuable supports. Discussing science and healthy debates with them really helped me to gain knowledge. Working with them made me learn a lot of new things and helped me to grow in the healthy environment. I cannot forget the help which I have got from the new lab members, Dr. Preeti Gupta, Vandana Sharma, Harsh Jog, Shailendra Kumar Chaube and Sunny Tiwari, Jesil, Jose, Rajath Sawant who supports a lot during the work.

In addition to the present lab members, I am thankful to all my former lab mates:, Dr. Debrina Jana, Mohit Raghuwansi, Rohit Chikkareddy, Sruthi Polali, Aswathy V.G., Sreyash Tandon, Sreeja Thampi and Abhijit Nayar.
My sincere thanks go to the Sanku Paul, Rabindranath Bag, Rohit Babar, Harshini Tekur, Gunjan Verma, Amandeep Sekhon, Jyoti Agrawal, Himani Rawat, Sunil Kumar, Nishtha Sachdeva, Sishir, SK. Rejaul, Amit Bhuniya, Aditi nandi, Aditya Mehra. I will never forget all the late night debates and discussions, games especially table Tennis (TT), which really make my hostel-life immensely joyful. I am really a lucky person who got such friends. During the Ph.D. program, I have got lot of technical and non-technical support. I thanks to Mr. Neelesh Dumbre, Anil Shetty, Mr. Prabhakar Anagare and Tushar Kurulkar for their constant support and helps to deal with paper-work. There are some people who always ready whenever you asked for help. I am thankful to the Nilesh Soni, Neha Khetan and Ayesha Fatima who always help whenever I asked them.
I acknowledge INSPIRE Fellowship, Department of Science and Technology (DST), India and IISER Pune for providing financial support during the period of research.
The most importantly, I thanks to my Mummy and Papa, Manvati Devi Nigam, Vineeta Devi Nigam, Neetu Rani Nigam, Khushbu Rani Nigam, Gyanvir Singh Nigam and Navneet Singh Nigam for their love and constant support and encouragement which always kept my morals high. Without their support, I will not be able to do any work.

Dedicated to my family...

Contents

Chapter 1

Introduction

Optical microscopy system has been used to investigate material characteristics, particularly imaging, light-scattering properties, light absorption and transparency of materials and much more. It was first utilized in 1660 by Robert Hooke for resolving the cork cell and hence he was able to discovered the cellular form of life [1]. In 1887, Robert Brown observed the random movement of pollen grains [2]. During the 16th and 17th century, scientists were enabled to investigate the matter and biological specimens in the micro-scale [3, 4] regime. The important thing is that light enables to observe things without altering the original forms. In 1873, the fundamental limit, diffraction limit, of the imaging resolution was formulated by Ernst Abbe which states that the spatial resolution of image observed using light cannot be more than, approximately, half of the wavelength of the incident light. This fundamental constraint restricts to obtain high-resolution images using optical fields. However, the researcher has harnessed microscopy tool with various techniques to observe important properties of matter and addresses the potential applications.
Microscopy system has been utilized for imaging of small specimens which include biological specimens, medical specimens for diagnostic purposes and nano-materials such as nanostructures of various kinds of materials. In the case of imaging, researchers have put an enormous effort to improve the spatial resolution so that the details of specimens can be analyzed.
In order to get rid of the diffraction limit, during the last two decades, several extraordinary methods were discovered and experimentally demonstrated, which helps to improve the spatial resolution down to the level of nanometer scale [5–17]. For these achievements, 2014 Nobel Prize in chemistry was given to Eric Betzig, Stefan Hell and William E. Moerner (for their pioneering research work in “super-resolution” fluorescence microscopy).

In addition to the imaging of specimens, the microscopy system has evolved with various important configurations such as upright and inverted microscopy, darkfield

microscopy, total internal reflection microscopy and dual-channel microscopy systems etc. which has been used for better optical resolution and give a platform to study furthermore optical phenomena. Among them, the configuration of dual channel microscopy system has been utilized in many important works such as the light scattering characteristics of novel nanostructure morphologies, transient absorption microscopy and spectroscopy [18–22], pump-probe technique for time–resolved studies for ultrafast processes [23–25] etc. The aforementioned techniques help to probe the light scattering from isolated nanostructures, heating effect of metal nanostructures, a lifetime of electronic and vibrational energy levels in nano-emitters (quantum dots, nanoparticles etc.) etc.

Among the emerging research fields, plasmonics is a rapidly expanding research area. The plasmonic nanostructure shows the unique optical properties where the optical fields can be manipulated at the sub-wavelength scales. Such properties enable to study optical fields beyond diffractions limit [26, 27]. To probe such important optical properties of the plasmonic nanostructure, it is necessary to develop optical instrumentation which can help to investigate complete optical information.

In this chapter, I have focused on the studies of light scattering characteristics of plasmonic nanostructures using advanced configurations of dual-channel Fourier optical microscopy and spectroscopy systems. This thesis describes the investigations of various nanostructure architectures, especially silver nanowire, nanoparticles and semiconductor mesowires systems, for their light propagation, localization, and emission behavior. In order to put the content of the thesis in a detailed way, I have started with a short introduction of important investigations performed using dual channel optical microscopy systems.

1.1 Dual channel optical microscopy system

The basic structure of dual channel system includes two objective lenses aligned opposite to each other in the vertical or horizontal configuration (shown in Figure1.1). This system is also called two channel system. In this system, the sample is placed at the common focal plane of both the lenses. Both the configurations have pros and cons which depend on the type of experiment. For example, the alignment of sample with respect to the focal plane is easy in a vertical configuration as compared to the horizontal configuration. However, if experimental conditions need rotation of sample w.r.t. the z-axis (normal to the sample plane), then horizontal configuration is good as compared to the vertical configuration.

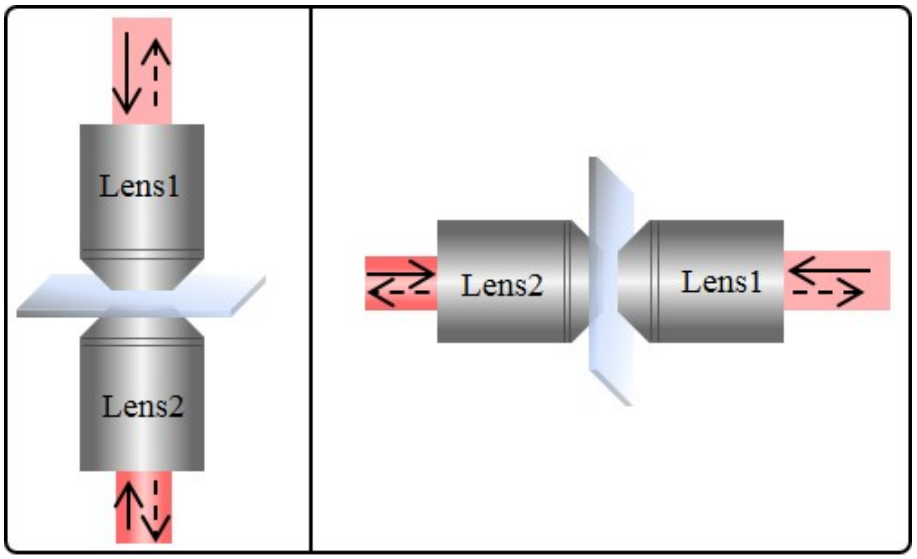

FIGURE 1.1: Schematic shows the dual-channel setup in two different configurations: vertical and horizontal. The both channels can be used for excitation and collection of light, respectively, as indicated by solid black and dashed arrows, respectively.

Such aligned lenses can be used for various purposes, for example, multiple excitations through the optically transparent substrate and/or from the superstrate. In the same way, to collect the scattered radiation from the sample, the same two lenses can be used and hence can collect possible maximum signals through the optically transparent substrate and from the superstrate. This configuration has been used for various observations such as spatial high-resolution optical imaging (especially axial resolution for better 3D imaging), temporal resolution for ultrafast processes and absorption cross-section for nanostructures etc. The following sections give detailed information about the observations of optical investigations performed using the dual channel configuration.

1.2 Dual channel system as a super-resolution microscopy tool

For the imaging of a specimen, the most important factor is the resolution, which reveals basic information about the morphological details of specimens. The most favorable tool is the light which works without any physical contacts with the specimens. While using light as a tool to observe any small (micro-nano) sized entities, there is a fundamental constraint, i.e., diffraction limit, on the spatial resolution of optical image. According to the Abbe's resolution criteria, the spatial resolution cannot be more than

the half of the wavelength of incident light. To overcome this problem, various solutions were raised such as confocal techniques [28–30], which essentially removes signals which are out-of –focus from the sample plane, structured illumination microscopy [8], scanning near-field optical microscopy (SNOM) [7] stimulated emission to deplete (STED) [31, 32], RESOLFT, SIM microscopy methods [33, 34] etc.
In order to further improve the lateral and axial resolution of optical image, it was necessary to modulate the point spread function (PSF) of focal spot of excitation beam. The PSF along optic axis was improved by illuminating with coherent counter-propagating wavefronts. It was performed with the help of two opposing lenses with two different configurations called 4pi and I^5M [35–38]. These two lenses focused the illumination light at the common focal plane. This optical condition formed multiple lobes along the optic axis as a result of interference, as shown in Figure1.2. The center lobe is quite bigger as compared to the side lobes. It is mandatory to remove these side lobes which contribute to the formation of ghost images in addition to the main image of the specimen.
By using this configuration, the resolution in axial direction was improved and achieved in the 100 nm range [36] which is three-to-seven fold improvement with respect to the existing single channel configuration. Figure1.2 shows the schematic of SWM, I^5M and 4pi setups with the PSF and OTF along the optic axis of illumination at the fixed wavelength, respectively. The comparative analysis of all these configurations indicates that the best performance is achieved from the 4pi microscopy system. Hence the better resolution improvements are attained because of full solid focusing angle of 4pi [39].

1.2.1 Dual channel configuration used for Pump-Probe technique for higher spatial and temporal resolution

Transient absorption microscopy and spectroscopy

In addition to imaging, the dual channel configuration has been harnessed for the study of absorption cross-section of nanostructures which has been used for imaging and spectral characterization. The above-mentioned optical techniques have been developed for highly-resolved spatial imaging of specimens. However, these techniques rely on the external markers such as dyes, quantum dots (exogenous), cellular auto-fluorescence (endogenous) fluorescent markers. Hence, the weakly fluorescent or non-fluorescent materials cannot be probed with the above mentioned developed microscopy systems. Most importantly, the use of external markers also affects the pristine behavior of specimens and perturbs the molecular and biological system especially when the system is smaller than the fluorescent markers [40]. In order to overcome this problem, the

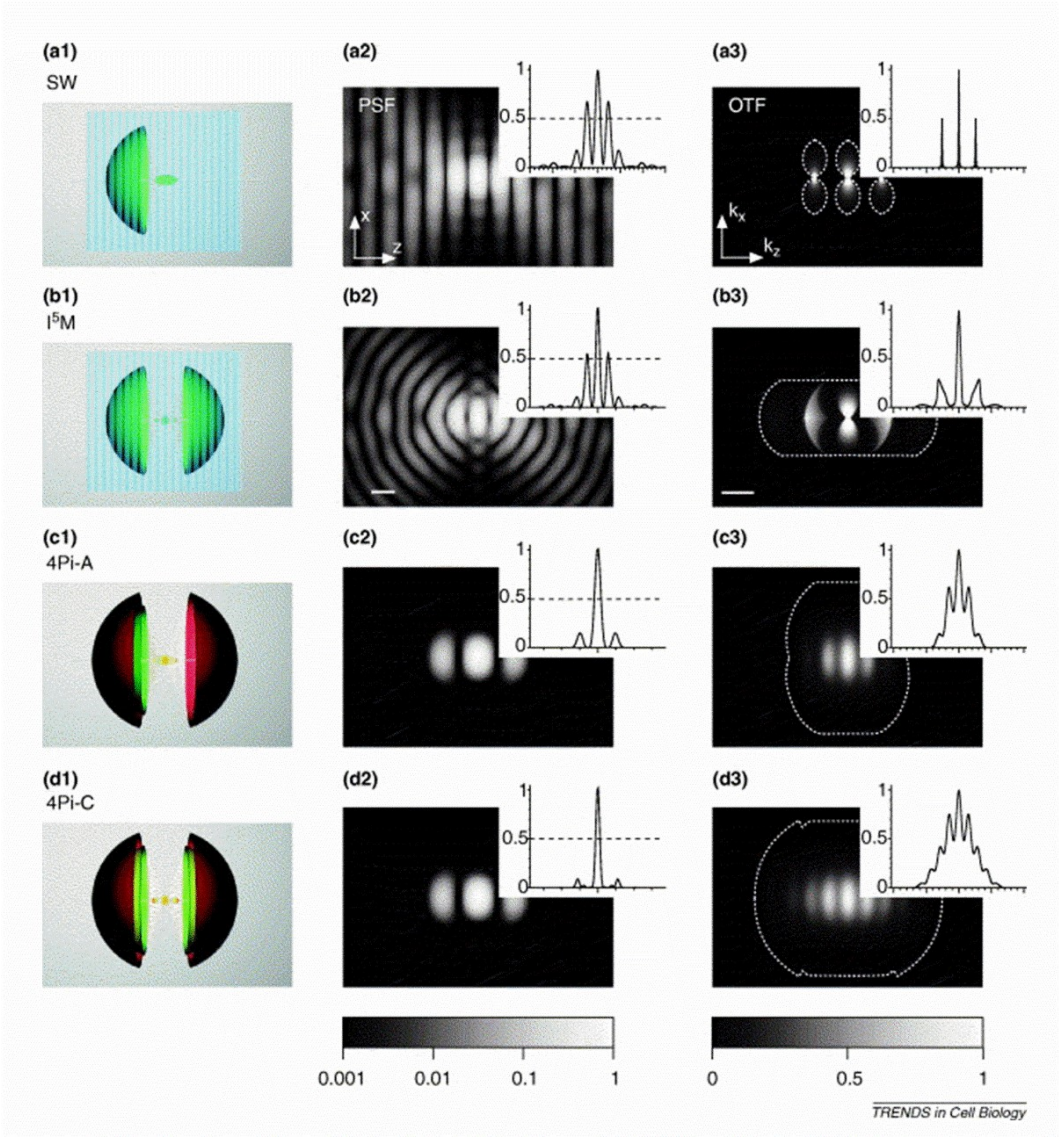

FIGURE 1.2: Shows the counter-propagating coherent wavefronts in microscopy configurations. The left-hand column (a1–d1) indicates the optical conditions of standing-wave microscopy (SWM), incoherent-illumination imaging microscopy (I^5M), 4Pi microscopy of type A (4Pi-A) and of the type C counterpart of the latter (4Pi-C). The center column (a2-d2) displays the effective point-spread function (PSF) of the corresponding microscopes, whereas the right-hand column (a3-d3) shows the corresponding amplitude of the optical transfer function (OTF). Reprinted with permission from [39].

pump-probe stimulated emission microscopy was introduced by S. Xie and coworkers [41].

The basic idea behind the transient absorption microscopy is the photo-induced absorption changes of a sample which can be utilized as a contrast mechanism for imaging. The experimental setup includes the two ultra-short pulses spatially overlapped in

the sample (illustrated in Figure1.3). The pump pulse excites sample and weak probe pulse interacts with the photo-excited sample as a function of delay-time τ after the pump pulse. The absorbance of two consecutive probe pulses, where one absorbs at the presence of pump pulse and other at the absence of pump pulse, is used to determine the pump-induced absorption changes for a given delay time. The more detailed information about the setups is given in the review articles [20, 21, 42, 43]. The transient absorption can be traced over a desired area of sample with the help of translational stage.

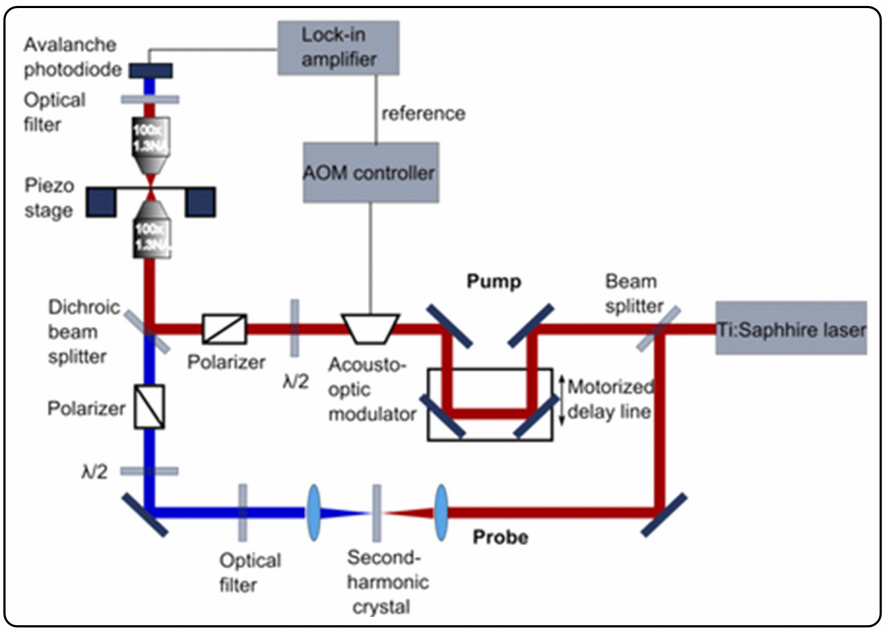

FIGURE 1.3: Schematic of experimental setup for transient absorption microscopy system. Reprinted with permission from [44].

Time-resolved studies for ultrafast processes

In addition to the imaging of nanostructure using pump-probe technique, this configuration is a vital solution to observe the ultrafast processes (sub-pico seconds) such as Auger recombination, charge carrier trapping [45], electron-phonon coupling and energy dissipation [46, 47] which cannot be studied here by using instrumentation like time-correlated single photon counting (TCSPC). Such instruments work on the principle of time correlation between excitation pulse and emission photons. Highly sensitive detector like APD, PMT etc is used to record very weak signals of emission from the sample for a small time duration. In addition to the high time-resolution, TCSPC will not be useful to study time-resolved processes with those specimens (or materials) with low emission quantum yield. Moreover, the emission based studies of nanostructures

are quite difficult when size goes beyond 20 nm because the emission efficiency is proportional to the square of volume of the nanoparticles.
All these problems can be overcome if we use the absorption properties of nanostructures. The efficiency of absorption based measurements increases with the decrease in size of the nanostructures. The pump-probe measurement of absorption becomes an excellent way to resolve ultra-fast processes which cannot be determined using TCSPC [48, 49]. The time scales of these processes depend on the size, shape and, most importantly, the surrounding environments which demand that the optical studies of nanostructures should be observed at the individual level.

Photo-thermal microscopy

The above sections describe the important uses of dual channel microscopy configuration for the spatial high-resolution imaging and time-resolved ultrafast processes in nanostructures which are not possible with the conventional microscopy setups. The emission based microscopy (Rayleigh scattering, fluorescence etc.) of molecules and nanostructures has dominated and become a standard technique.
In contrast to the fluorescence-based microscopy methods, photo-thermal contrast arises by releasing photo-induced heat from nanostructures [50, 51]. This heat increases the local temperature and alters the refractive index of the vicinity of absorber (specimen). The change in the refractive index of vicinity can be detected by optical techniques such as photo-thermal heterodyne detection [52, 53], differential interference contrast [54]. The experimental setup of photo-thermal microscopy is shown in Figuree1.4.

The sensitivity of these methods reaches the level of single molecules [56, 57]. The mentioned methods use the dual channel technique where one channel is used to heat nanoparticle by illumination (as a pump) of wavelength with higher absorption value and another channel is used (for probe) to see the change in the vicinity of the nanoparticle.

Till now, I have explained about the dual channel microscopy system and its uses in various important observations of optical phenomena which are not possible with the conventional microscopy system. In addition to the above-mentioned optical investigations, we have used this system to study further optical properties of plasmonic nanostructures and 2D materials. In this thesis, I have focused on the development of dual channel microscopy and spectroscopy systems to probe the light localization, propagation and emission behavior of one-dimensional nanostructures. In order to understand the observed new studies of isolated and hybrid nanostructure systems, it is important to understand the plasmonic behavior of nanostructure systems.

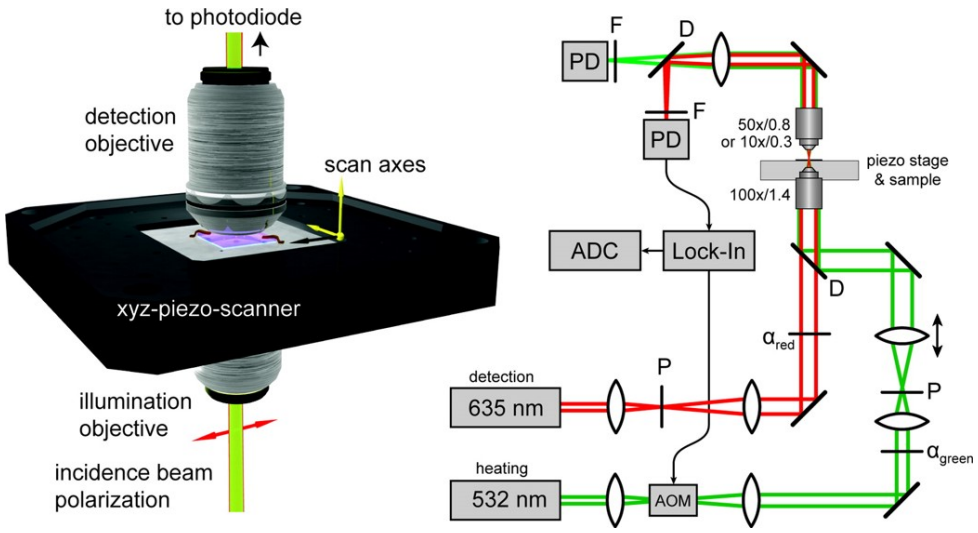

FIGURE 1.4: Shows the dual channel experimental setup for photo-induced heat imaging of nanoparticles: PD, photodiode; P, pinhole; D, dichroic mirror; F, filter; AOM, accusto-optic modulator; α, variable ND filter; ADC, Adwin analog-digital converter. Reprinted with permission from [55].

1.3 Light localization, propagation and emission in plasmonic nanostructure systems

Plasmonics is a newly emerging field of optics which shows interesting possibilities in various important areas. It exploits the unique ability of metallic nanostructures to modulate the optical field at sub-wavelength scales. Such manipulations are possible by the collective oscillations of free electrons at the surface of metals. It enables the light-confinement and propagation beyond the diffraction limit with the help of localized surface plasmons (LSP) and surface plasmon polariton (SPP) [26, 27]. These important manipulation of light in nanometer dimension opens up numerous applications which include plasmonic-based devices and optical components below 100 nm scale [58–62], enhanced light-matter interaction enables improvement in molecular spectroscopy techniques [63–67], a sensor for bio and molecular detection [60, 68–70]. This unique property also helps in the development of novel techniques for high-resolution microscopy system, plasmonic nanolasers etc. [71–75].

In addition to the various optical properties of plasmonic nanostructures, few important properties are the light confinement (localization), propagation and emission. The modulation of these properties plays a critical role in shaping plasmonic devices. One such plasmonic device is an antenna which works on the basis of light localization and directional emission. The plasmonic nanostructures show the capability of light localization and emission which has directional nature and hence act like an optical antenna

which has the capability to work in a visible spectrum of light [76, 77]. Therefore, it is important to modulate and generate new kind of geometry of nanostructure to harness the capability of antenna properties. In order to understand the localization, propagation, and emission of light, it is important to understand the phenomena which enable all these controls of light.

1.4 Surface plasmons

The surface plasmons were first observed by measuring the energy losses of fast electrons through the thin metal film [78]. Pines and Bohm have also shown that the long range of coulomb interaction between valence electrons of metals exhibits collective oscillations [79, 80]. After a couple of years later, Powell and Swan demonstrated experimentally the existence of collective oscillations by doing series of electron energy-loss experiments [81, 82], and quanta of these oscillations were named as surface plasmons [83]. Thereafter, this vital optical property of metal nanostructures was further studied and described in the various ways. The surface plasmons are associated with localized field and propagation of energy which is called as localized surface plasmons (LSP) and surface plasmon polaritons (SPP). The detailed description of these quantities is given in next few sections along with the implications in various important applications.

1.4.1 Localized surface plasmons (LSP)

The localized surface plasmons are associated with the resonant electromagnetic behavior in the metal nanoparticles which arises because of resonant oscillations of free conduction electrons within a particle volume [27, 84]. Schematic representation is shown in Figure1.5 where a particle with diameter $d << \lambda$ illuminated with light of wavelength λ drives the collective oscillation of conduction electrons. The incident oscillating field is coupled to the collective oscillation of conduction electrons, energy coupled into the LSP mode. When the frequency of incident field matches with the natural oscillation frequency of electrons, then it is called resonant frequency and called as the LSPR mode. Hence, when it is LSPR mode, strongly enhanced homogeneous field is built up in the vicinity of nanoparticle system. This leads to the enhancement in the absorption and scattering cross-section of electromagnetic waves. The optical properties associated with the frequency of oscillation (LSP) is highly sensitive to the material of nanoparticle, morphology of nanostructure and surrounding medium [85–89].

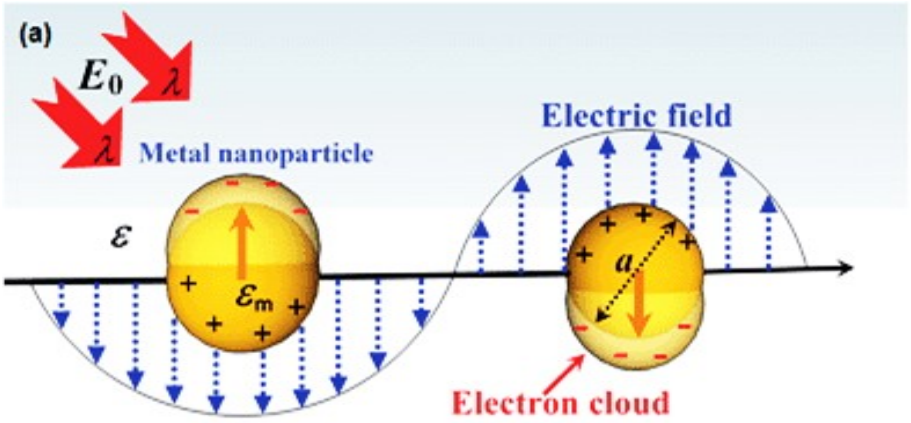

FIGURE 1.5: Shows the schematic of collective oscillation of conduction electron charge cloud relative to the nuclei with applied oscillating electric field. Reprinted with permission from [85].

1.4.2 Surface plasmon polariton (SPP).

The collective oscillations produce enhanced electric field in the vicinity of surface of the nanostructures. This enhanced field can also be observed at the planar interfaces between metal and dielectric medium. The coupled electromagnetic field with the surface plasmons gives rise to the modes which propagate along the interface and are known as surface plasmon polariton (SPP) [90, 91]. These surface electromagnetic waves propagate along the interface with damping due to the radiative and non-radiative decays. The magnitude of electric field decays exponentially along the normal to both the mediums [92], as shown in Figure1.6. The momentum wavevector of these surface waves is always greater than the exciting electromagnetic field with same frequency. This fact can be understood from the dispersion relation of SPP (shown in Figure1.8).

1.4.3 Surface plasmon polariton (SPP) assisted light propagation in plasmonic nanowires

The metal nanowires support surface plasmons polaritons which are electromagnetic surface modes excitations associated with the charge density waves at the surface of metallic systems or metal-dielectric interface. Such modes do not couple directly to free-space radiation and hence need appropriate coupling mechanisms for the excitation or decay into free photons. To develop a better understanding of these modes, it is important to analyze it theoretically. In order to calculate the surface plasmons eigen modes of thin wires, we need to solve the homogeneous wave equation with taking into

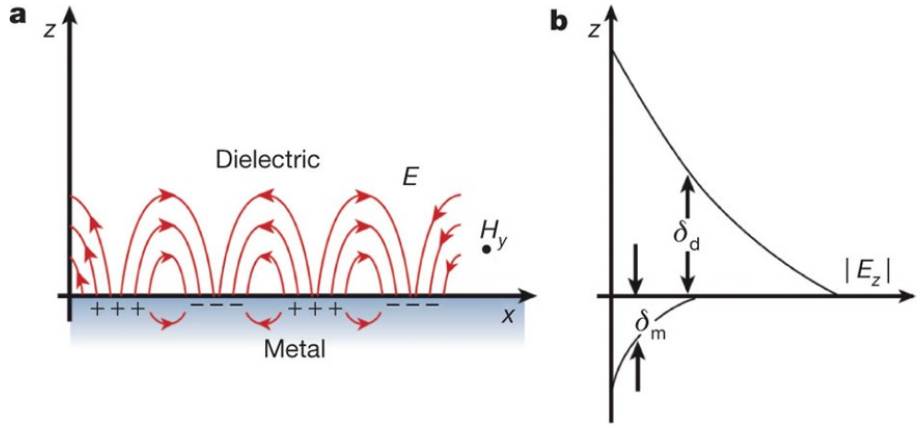

FIGURE 1.6: (a) shows a collective excitation at a metal–dielectric interface. The electromagnetic field (electric field, E, z- x plane; magnetic field, H_y, y direction) is drastically enhanced at the interface. (b) The electric field profile across the interface which decays exponentially with a characteristic length δ_d (of the order of the wavelength of incident light) in the dielectric and a characteristic length of δ_m (the skin depth) in the metal. Reprinted with permission from [93]

account the proper boundary conditions [94].

$$\bigtriangledown \times \bigtriangledown \times E(r,\omega) - \frac{\omega^2}{c^2}\epsilon(r,\omega)E(r,\omega) = 0 \tag{1.1}$$

For the calculations of thin wire, let us consider a cylinder, which is oriented along z- axis, of radius R, dielectric permittivity ϵ_2, as shown in image Figure1.7. The dielectric permittivity of surrounding medium of wire is ϵ_1. Here, Re $\epsilon_1 > 0$ and Re $\epsilon_2 < 0$, indicates the negative dielectric permittivity of metal and positive for surrounding medium. The negative dielectric permittivity of metal system plays critical role for the formation of these confined modes.

For the calculations of electric field profile of surface modes, we can use the method of separation of variables to the Maxwell equations in each medium [95, 96].
In cylindrical coordinates, the electric field distribution in each medium is given by

$$E_i(r) = \epsilon_{i,m}E_{i,m}(k_{i,\perp}\rho)e^{-im\varphi}e^{ik_{||}z} \tag{1.2}$$

Where $i = 1, 2$ indicates the regions outside and inside of the cylinder, respectively. Here, $k_{||}$ is the longitudinal wave vector and k_o is vacuum wave vector, $k_o = \frac{\omega}{c}$ and $k_{i\perp}$ is the transverse wave vector in i medium. Here, m denotes an integer characterizing the modes. The relation between longitudinal, transverse and vacuum wave vector is given below :

$$\epsilon_i k_o^2 = k_{||}^2 + k_{i\perp}^2 \tag{1.3}$$

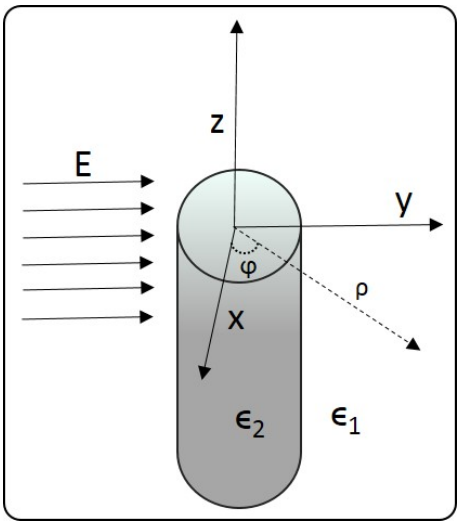

FIGURE 1.7: Schematic of a nanowire (cylindrical model) oriented along z- axis. Cylindrical coordinate system were used for the calculation of electromagnetic modes in metal cylinder.

In the equation 1, the $E_{i,m}$ represents the normalized electric field in the medium inside and outside and with m modes. Similar expressions hold for magnetic field H (see the appendix A for detailed expressions of E and H).
The vacuum wavelength and wave vector is given by

$$\lambda = \frac{2\pi}{k_o} \tag{1.4}$$

The wave vector and wavelength in i medium is given by

$$k_i = \sqrt{\epsilon_i} k_o \tag{1.5}$$

Where, $\sqrt{\epsilon_i}$ is refractive index of i medium.

The longitudinal component of wave vector is greater than the wave vector in dielectric $k_{||} > k_1$ which makes the perpendicular component, $k_{i\perp} = \sqrt{k_i^2 - k_\perp^2}$ is imaginary which means the plasmons modes are nonradiative and confined near the metal/dielectric interface. For the transverse confinement, the length scale is given by $\sim \frac{1}{\sqrt{k_i^2 - k_\perp^2}}$. The dielectric function of metal cylinder has an imaginary part which leads to the losses (heating) at optical frequencies. Therefore, it gives the dissipation as the plasmons propagate along the nanowire. This defines the propagation length of surface plasmons polaritons of metal nanowires. The dissipation of plasmons varies as a function of size of the nanowires and surrounding temperature [97].

Allowed modes in nanowire

The metal nanowire supports electromagnetic field modes which is also depends on the dimension of geometry. Here, I have explained the allowed plasmon modes in nanowire cylindrical geometry. In order to understand the allowed modes, we have to solve the mode equation given below:

$$\frac{m^2 k_{||}^2}{R^2}\left(\frac{1}{k_{M\perp}^2}-\frac{1}{k_{D\perp}^2}\right)=\left[\frac{1}{k_{D\perp}}\frac{J_m'(k_{M\perp}R)}{J_m(k_{M\perp}R)}-\left[\frac{1}{k_{D\perp}}\frac{H_m'(k_{D\perp}R)}{H_m(k_{D\perp}R)}\right]X\left[\frac{k_M^2}{k_{M\perp}}\frac{J_m'(k_{M\perp}R)}{J_m(k_{M\perp}R)}-\frac{k_D^2}{k_{D\perp}}\frac{H_m'(k_{D\perp}R)}{H_m(k_{D\perp}R)}\right]\right. \tag{1.6}$$

The above equation gives the allowed values of $k_{||}$ as a function of m, R and ϵ_i. The detailed derivation of the above equation (mode equation) can be see in Appendix A.

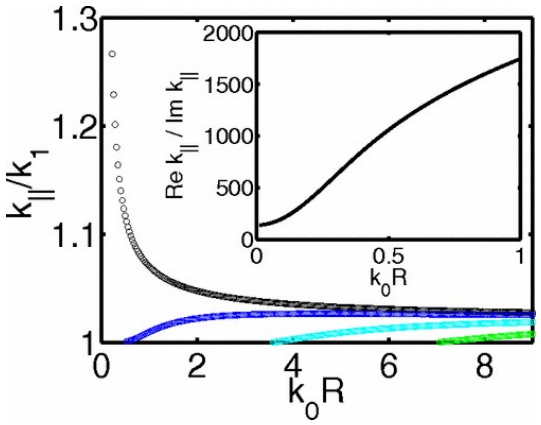

FIGURE 1.8: Above plot represents the plot of $k_{||}$ as a function of allowed plasmons modes and R (radius of wire). The inset shows estimate of propagation losses as a function of radius R. Reprinted with the permission from [94]

As illustrated in Figure1.8 (plot of allowed wavevectors $k_{||}$, as determined by mode equation), we can see that the all modes are not supported. Modes $m = 0, 1, 2, 3$ have different variations with respect to the diameter of nanowire. The modes, $\mid m \mid \geq 1$ have cut-off values as wire-radius tends to 0 . Below these values, such modes does not exist. As we can observed from the graph, the $m = 0$ mode (fundamental mode) exhibit a unique behaviour where $k_{||} \propto \frac{1}{R}$. This implies that the field outside medium of wire is tightly localized around the wire with the scale of R. Specifically, this modes allows the field confinement well below the diffraction limit. This mode can be visualized as charge density surface waves along the wire. The detailes analysis of these modes can be see in appendix A.

Coupling of SPP with light

As mentioned above, for a given energy , the wave vector of SPP is always greater than the wave vector of free space radiation. This can be observed from the plasmons dispersion curve and light-line, shown below (Figure1.9).

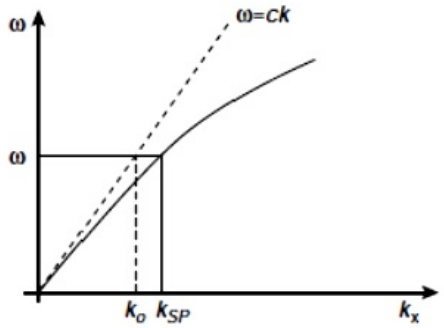

FIGURE 1.9: Shows the dispersion curve of SP mode (solid black line) and free space electromagnetic radiations (dashed black line). It shows the momentum mismatch between wave vector of SPP and light for a given frequency. Reprinted with permission from [88].

To bridge the gap of momentum mismatch between the wave vectors of SPPs and free-space electromagnetic waves, it is necessary to make arrangement in such a way that the momentum mismatch can be bridged between momentum of free radiation and SPPs [92]. In order to solve the requirement of momentum mismatching, there are various methods that have been developed such as grating coupling, prism coupling and laser light focusing at the geometrical discontinuities.

Prism coupling

One of the solutions of excitation of SPPs is the evanescent waves. The evanescent wave can be generated at the interface between dielectric medium with refractive index n > 1 and air. In this case, the light line is tilted by a factor of n and $\omega = \frac{ck}{n}$. Hence, this can be done using prism in two possible ways: Otto configuration and Kretschman configuration.

Otto Configuration

This configuration consists of a prism which is used to create evanescent waves. The tail of the created evanescent waves is then used for exciting SPPs [98]. There is a dielectric (n1 < n) gap between prism and metal medium. This configuration is relatively difficult since keeping medium with optimum thickness between glass and metal surface is difficult.

Kretschman configuration

In this method, the thin metal film is deposited on the top of the prism without any gap. Hence, this configuration gives two interfaces: metal/glass and metal/air. To generate SPP at the metal-air interface, an evanescent wave was created at the metal-glass interface which penetrates the deposited thin film. The film thickness plays a critical role here. If the film thickness is too thin, the SPPs will be damped strongly because of radiation damping into the glass. If metal film is too thick then the SPP cannot be efficiently excited at the metal-air interface [99].

Grating coupling

In order to overcome the above problems with the prism coupling, for efficient excitation of SPPs, the alternative way is grating [92, 100]. Here, the metal surface is structured with the right spatial periodicity in such a way that it can add extra momentum to the free space wavevector which matches with the wave vector of SPPs. The new parallel wavevector will be $k_x^{'} = k_x + \frac{2\pi n}{a}$, where $\frac{2\pi n}{a}$ is a reciprocal-lattice vector of grating.

Tightly focused laser light

This method is generally used to excite SPPs in the case of geometrical discontinuities in the nanostructures such as the end of wire and strips, edges and corners of plates etc. In this configuration, the light is illuminated with a tightly focused laser beam using the high numerical aperture objective lenses.

1.4.4 Emission behavior: Antenna properties of nanostructure system

Previous sections briefly explained about the sub-wavelength light localization and propagation properties of plasmonic nanostructures. These plasmonic nanostructures are not limited to localization and propagation of light. It also emits light which is directional in nature. This important property opens up a new direction for research and applications. One such important and promising application is an antenna which used to manipulate electromagnetic field between localized sub-wavelength field and free radiation. Such devices (nanostructures systems) can be used to transfer energy between localized sources which can be receiver or transmitter and free radiation [76, 77]. The field scattered from the nanostructures such as nanowires, nanoparticles, and hybrid

nanostructure system can be used as a light source and optimized for directional emission (shown in Figure1.10(b)). In addition to the directional emission by plasmonic nanostructures, these nanostructures can also influence the emission of fluorophores by placing them in the vicinity of plasmonic nanostructures. The spatial re-direction of emission from the molecules/fluorophores is modified because of coupling between fluorophores and plasmons which form plasmophores and hence radiates in the direction which is governed by plasmon modes. Figure1.10(a) shows an example of an optical Yagi-Uda antenna where a quantum dot was coupled to the feed of the antenna. The emission of quantum dot was in resonance with the feed element of Yagi-Uda antenna, the resulting quantum dot emission was strongly polarized and highly directed into a narrow forward angular cone [101]. Such modification in the directional emission of the fluorophore is advantageous because of emission enhancement which further increases the detection efficiency of detectors by placing detectors in the direction of emission [101–103].

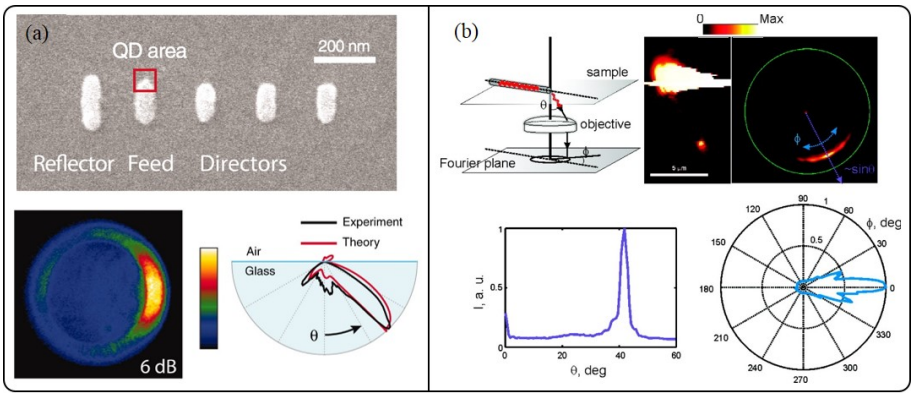

FIGURE 1.10: The directional emission from the plasmonic nanostructures. (a) shows the directional emission of coupled quantum dot with the Yagi-Uda antenna. (b) represents the directional emission from the end of silver nanowires. Reprinted with the permission from [101, 104].

1.5 Scope and outline of the thesis

This thesis addresses the development of dual channel Fourier optical microscopy and spectroscopy instrumentation and probing the optical properties of plasmonic and hybrid nanostructure systems. In particular, the work is focused around the light localization, propagation, and emission from the sub-wavelength nanostructures which show the implications in some important applications such as optical antenna, sub-wavelength waveguides etc. The content of the thesis includes the home-built instrumentation and

optical properties of nanostructures. For a general overview, the following is elaborate content about the next chapters.

1.5.1 Chapter-2

Here, we explain experimentally studied surface plasmon polariton assisted light propagation in serially coupled silver nanowire (Ag-NW) systems. We describe the relation of bending angle between the nanowires and light propagation through it. From this study, we observed that obtuse angles between the nanowires arms of coupled wire system resulted in better transmission than acute angles. We also experimentally observed that by varying incident polarization of excitation light, the light emission from junction and distal ends of Ag-NW dimers can be systematically controlled. Furthermore, we show the light routing and polarization beam splitting capability in the obtuse-angled Ag-NW dimer.

1.5.2 Chapter-3

The main focus of this chapter is to show experimentally how a single Ag nanoparticle (NP) coupled to an Ag nanowire (NW) system can be used for directional emission of photons. By employing dual-excitation Fourier microscopy with spatially filtered collection-optics, we present the single- and dual-directional out-coupling of light from NW-NP junction for plasmons excited through glass-substrate and air-superstrate. Furthermore, we have also observed how the NW-NP junction can influence the directionality of molecular fluorescence emission, thus functioning as an optical antenna. The results discussed herein indicate the potential applications in realizing directional single photon sources and also a promising quantum plasmon circuitry.

1.5.3 Chapter-4

Herein, we explore the directional nature of emission from an organic waveguide through substrate (glass) and superstrate (air). The waveguide was excited at one end and the propagated light was out-coupled from the distal end which was collected through the two different medium i.e glass substrate medium and from air-superstrate. The scattering properties of nanostructures alter when the surrounding medium is anisotropic. This study explains the spatial profile of far-field emission in the two different media. In addition to the far-field imaging, the spectral characteristics of emission into the two mediums were also recorded. We could find the significant changes in the spectrum of Fabry-Perot modes for these two mediums.

1.5.4 Chapter-5

This chapter mainly describes the summary and future directions of the research work presented in the thesis. By employing the dual-channel Fourier optical microscopy and spectroscopy system, we have been working on the studies of linear and nonlinear optical properties of nanostructures. In addition to the high-resolution imaging, this instrument also shows a good platform to study the far-field profile of scattering in nearly 4pi solid angle of observation. This helps to control the emission properties of the nanostructure systems. The dual channel architecture can be extrapolated to study energy-momentum spectroscopy which further provides the information about the wavelength dependent emission profile.

Chapter 2

Light Propagation and Emission in Conductively Coupled Silver Nanowire Geometry

Chapter 2 is an adaptation of the research article '*APPLIED PHYSICS LETTERS 101, 111111 (2012)*'. The article describes the propagation of light in serially coupled plasmonic nanowire dimer with geometry dependence and polarization control.

2.1 Introduction

How to propagate and localize light at subwavelength scale? These are important question in nanophotonics [105–107] and has great relevance in realizing nano-circuits of light. In dielectric optics, diffraction of light has been a major hindrance to control light at nanoscale, but in recent years metallic nanostructures that support surface plasmons [108, 109] have opened up new avenues to propagate and localize light at subwavelength regime [110]. This has led to tremendous interest in interaction of light with nanoscale plasmonic geometries [108, 111], such as silver nanowires [112], that can be harnessed as circuit-element in a nanophotonic circuit. For such circuits to emerge it is necessary to further develop and understand capability of plasmonic nanowires to perform various logical functions similar to circuit elements in electronics. In the context of plasmonic nanowire circuits, there are certain issues that need to be probed and understood, such as: the capability of plasmonic nanowires to transmit light from one nanowire to another; the effect of nanowire coupling on propagation of light; the ability to control the fan-out in coupled nanowire systems.

Motivated by this requirement, herein we study the light transmission and emission in a specific plasmonic nanowire system: self-assembled, end-to-end coupled silver nanowire (Ag NW) dimers with a certain bending angle between them. The objective of this study was two-fold: (1) to find the effect of bending angle between the silver

nanowires on surface plasmon polariton-assisted light propagation; (2) to control the intensity of light emission at the junction and distal ends of the Ag NW dimer via polarization of incident light. As a consequence of polarization control, we also showed capability of Ag NW dimer to route light and act as polarization beam splitter. Ag NWs have been previously studied in the context of nano-waveguides [112–120], optical logical gates [121], quantum optics [113], surface enhanced Raman scattering (SERS), [119, 122–124], colouring fluorescence emission [125], chiral plasmons [126] etc., indicating their versatility as nanophotonic element.

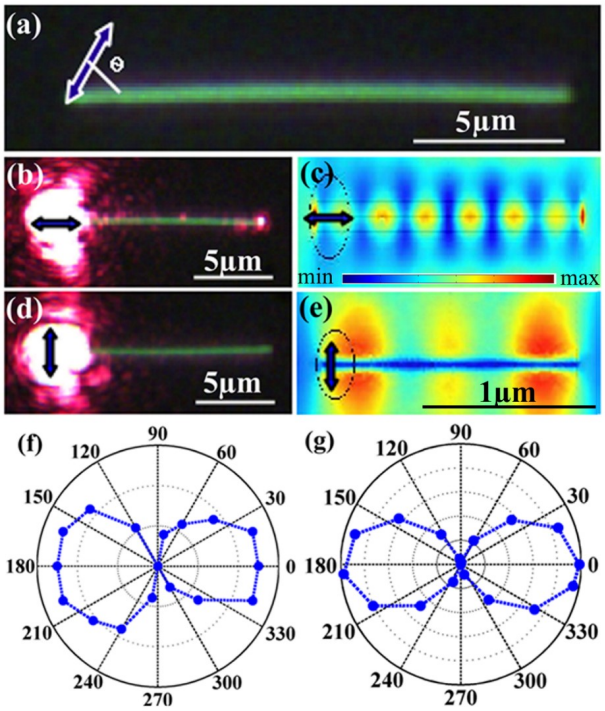

FIGURE 2.1: (a) Optical image of an isolated Ag NW with specific angle convention. The arrow indicates the electric field polarization. The $m = 0$ mode leads to light emission at the distal end of the Ag NW. The (b) experimental and (c) simulation results for $m = 0$ mode. The $m = 1$ mode does not result in the emission of light at the distal end of the Ag NW. The (d) experimental and (e) simulation results for $m = 1$ mode. (f) Experimental and (g) simulation results of emission at the distal end of Ag NW as function of input polarization angle.

The SPPs of Ag NW can be excited in two fundamental modes i.e. $m = 0$ and $m = 1$ and a linear combination of both of them as a function of incident light polarization. We have studied the light propagation in Ag NW by exciting $m = 0$ and $m = 1$ modes, respectively. In Figure2.1a, we show an optical image of single isolated Ag NW used in the experiment. Figure2.1b and c show the experimental and simulation using 3-D finite element method of $m = 0$ mode configuration. Clearly, our data indicated bright

emission at the distal end of the Ag NW, whereas for $m = 1$ mode, our experimental (Figure2.1d) and simulation (Figure2.1e) results showed no emission at the distal ends of the Ag NW. In Figure2.1f and g, we have shown the polar plot of the experimental and simulation results of the variation of emission intensity at the distal end of the Ag NW as a function of input polarization, respectively.

2.2 Preparation of Silver nanowires

Our preparation method was based on seed-mediated growth technique developed by Xia and co-workers [127]. Briefly, we prepared two solutions A and B, in which A was 0.087M $AgNO_3$ (Sigma-Aldrich) in 3ml of ethylene glycol (EG) and solution B was 0.435M poly (vinyl pyrolidone) (PVP) in 3ml of EG, both at room temperature. The molarity ratio of A and B was kept 1:4. These two solutions were injected by a two-channel funnel simultaneously to 5ml of EG, which was preheated at 160^oC, at the rate of 0.3ml per minute. Here, the rate of injection plays a critical role in the formation of nanowire geometry. After completely injecting the whole solution, the final solution was left for stirred and heating at 160^o C for about an hour. Thereafter, the cooled final solution was centrifuged at 2000 rpm for 10 min and was washed five times with ethanol to remove EG and PVP (surfactant) and 10 times with water to remove unwanted spherical nanostructures. During the washing of the suspension of AgNW, it was also sonicated for 5min. duration.
Figure2.2 illustrates the reaction mechanism of the formation of coupled Silver nanowires. The sonication of centrifuged silver nanowire plays a potential role for making conductively coupled nanowire dimers. For the optimum duration of sonication can give you a good number of yield of this kind of geometry. The long duration of sonication can break the nanowires into smaller rods. The as-prepared nanowires were further characterized using a high-resolution transmission electron microscope and optical microscopes.

2.2.1 Characterization of serially coupled silver nanowire

The end-to-end coupled nanowire was characterized using various imaging tools such FESEM, HRTEM, optical microscopy etc. The following section gives the morphological information about this geometry. The optically found, using an optical microscope, the coupled nanowires on the drop-casted well disperse Ag NWs. Figure2.3 shows the optical darkfield images of conductively coupled Ag NWs with various configurations. Figure2.3 (a-c) shows obtuse angle geometry where angle is defined in between the two arms of nanowires. Figure2.3 (d-f) represents the acute-angle coupled nanowires.

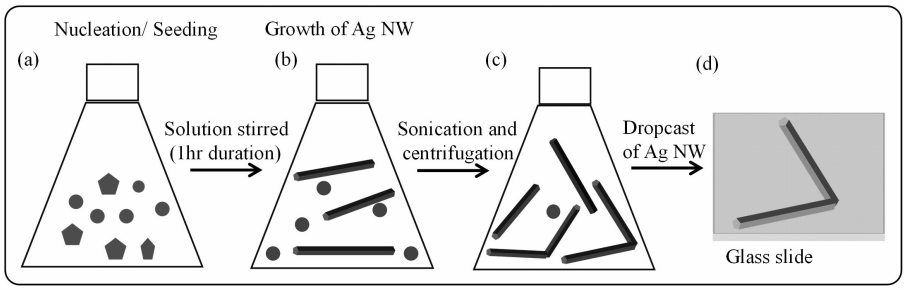

FIGURE 2.2: Schematic shows the synthesis process of end to-end-coupled Ag NW (a) Nucleation occurs after formation of silver clusters. (b) Growth of seeds into nanowires and various other shapes of nanostructures (nanoparticles, nanocubes, nanorods etc). (c) To remove small unwanted particles and other impurities, the solution is sonicated followed by centrifugation. (d) A small drop of Ag NW suspension drop-casted on a cleaned glass substrate.

The synthesis method could not reveal the control over these geometries and hence it is a random process. Using the high-resolution imaging techniques (HRTEM), we have figure out the junction morphology of this geometry. It was found that the wires were attached to each other without any interface or any other medium, shown in Figure2.4(b) and (d).

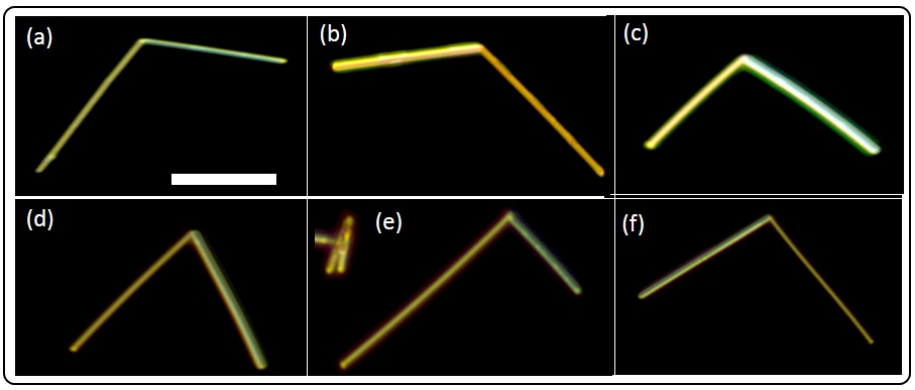

FIGURE 2.3: Dark-field microscopy images of a variety of isolated Ag NW dimer. (a-c) shows the obtuse angle nanowire geometry and (d-f) shows the acute angle geometry of nanowires. Scale bar of the images is 5μm. The total lengths of the Ag NW dimers were around 15 microns.

In this study, we employ an end-to-end coupled Ag NW dimer and investigate their plasmon-mediated light propagation and emission properties. The advantage of this serial coupling configuration is that minimal area of the nanowire is utilized for connection, thereby leaving the lengths of the nanowire for further utility and coupling. This unique geometry can facilitate light propagation along the nanowires and localization at the nanowire junctions on a single nanophotonic platform [119], and hence very

useful in building nano-plasmonic circuits.

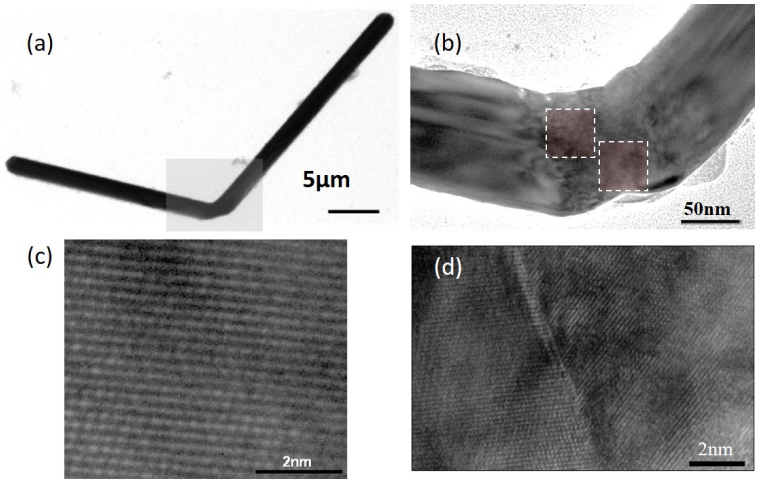

FIGURE 2.4: (a) HRTEM image of single Ag NW ; (b) HRTEM image shows connection of two Ag NWs; (c) Shows the high-resolution image of one arm (indicated by white dashed rectangle) of coupled Ag NW; (d) high-resolution image of junction (indicated in white dashed rectangle) of coupled Ag NW at 2nm scale.

2.3 Optical measurement of light propagation in serially coupled Ag NW

2.3.1 Instrumentation setup for optical measurement

Self-assembled Ag NW dimers were prepared as per the protocol discussed before [119]. The schematic of the optical layout used in our work is shown Figure2.5. For optical probing of Ag NW dimers, the solution containing Ag NW dimers were drop-casted on a glass slide which was pre-cleaned (with detergent and rinsed with deionised water, and then wiped with acetone and methanol to remove some inorganic impurities). The drop-casted solution was spread over the cleaned glass slide and dried at room temperature in a dust-free environment. The as-prepared glass slide was transferred onto a computer controlled stage of an upright microscope (Olympus BX-51) attached with a CCD camera at one of the output ports. Using this microscope system, the deposited Ag NW dimers were spatially identified by bright-field and dark-field images.
Further, an expanded laser (632.81nm, He-Ne laser) was sent through a polarizer (to control the input polarization) and was further coupled into the objective lens (0.9 NA, 100X) of the microscope. The laser spot (1 to 2 microns in diameter) was carefully focused either at the end or at the junction of the Ag NW dimer. The backscattered light

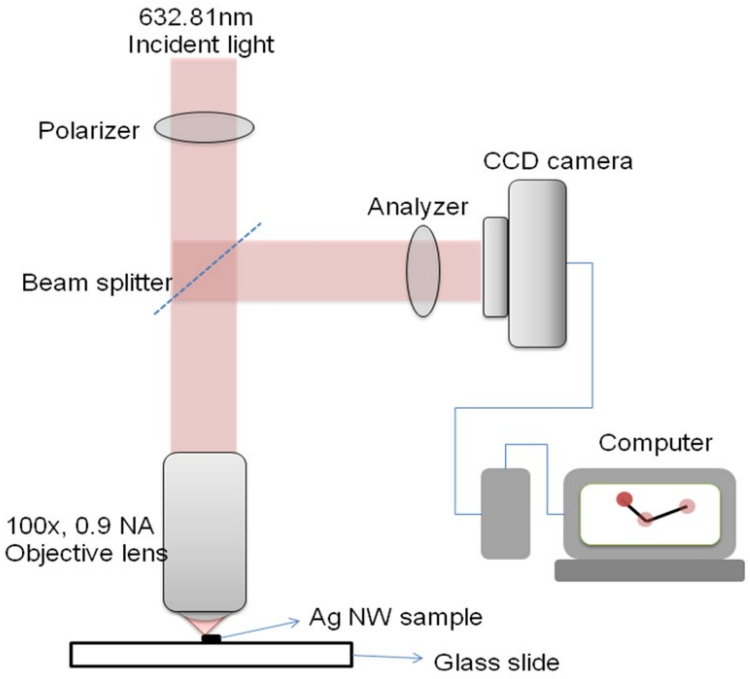

FIGURE 2.5: Schematic of the optical layout used in the experiments.

was collected via the same objective lens and was further guided towards a polarization analyzer (to examine the emitted polarization from nanowires) and then imaged on a CCD camera.

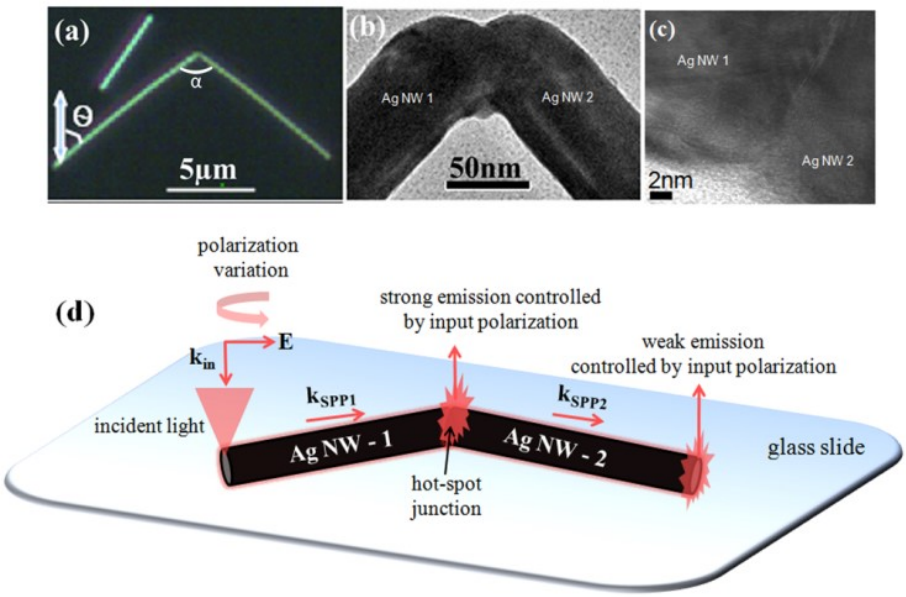

FIGURE 2.6: (a) Optical image of a silver nanowire dimer; (b) transmission electron microscopy image of the silver junction; (c) high-resolution transmission electron microscopy image of the silver nanowire junction; (d) schematic of the experiment to show polarization controlled emission at junction and distal ends of Ag NW dimer.

2.3.2 Geometry dependent light propagation in serially coupled Ag NW

In order to test the plasmon-assisted light propagation, we utilized one of the isolated Ag NW dimers that were connected in an end-to-end configuration. Figure2.6a shows a representative optical image of an end-to-end connected Ag NW dimer. To confirm that the two ends of the Ag NW are connected to each other, we recorded transmission electron microscopy image at two different resolutions as shown in Figure2.6b and c. We clearly observed the conductively coupled ends of the Ag nanowires. This physical connection is critical for plasmons to tunnel from one nanowire to another of coupled wire. Also, the junction between the nanowires, which can be essentially considered as a defect in the geometry (see Figure2.6c), is a plasmonic hot-junction for surface enhanced optical spectroscopy [119].
The schematic in Figure2.6d shows the experimental configuration. A laser beam (632.81nm) was linearly polarized using a $\frac{\lambda}{2}$ plate and focused through a high numerical aperture objective lens at one end of the Ag NW dimer and emitted light intensity at junction and distal ends of the NW dimers were studied. There are two important parameters in our experiment: first is the bending angle (α) between the Ag NW dimer, and the second one is the polarization of incident light (θ). First, we probed the angle dependence followed by polarization dependence.

In order to optimize the design parameters of nano-optical waveguides, it is important to characterize the bending and coupling losses [118]. In plasmonic nanowire waveguides and networks [117], there is an intricate relationship between the geometrical coupling between nanowires and propagation characteristics of SPPs. In the context of light propagation, we found an interesting trend in our Ag NW dimer system. The Ag NW dimers that we studied were prepared by a bottom-up approach, and the formation of the dimer geometry is essentially a thermodynamically-driven self-assembled process.
It was interesting to note that for almost all the Ag NW dimers that we observed during the course of experiments exhibited a sharp bending angle between the Ag NW which was either acute or obtuse (see sample dark-field optical images in Figure2.3). We were interested in probing the dependence of this bending angle (α) on the SPP-assisted light propagation in our Ag NW dimers. We observed that whenever the bending angle between the Ag NW dimer was acute ($\alpha < 90$), as shown in Figure2.7a, we evidenced intense light emission at the junction, and very negligible emission intensity at the distal ends of the Ag NW dimer. In contrast, when the bending angle between NWs was obtuse ($\alpha > 90$), as shown in Figure2.7b, we observed greater emission intensity at

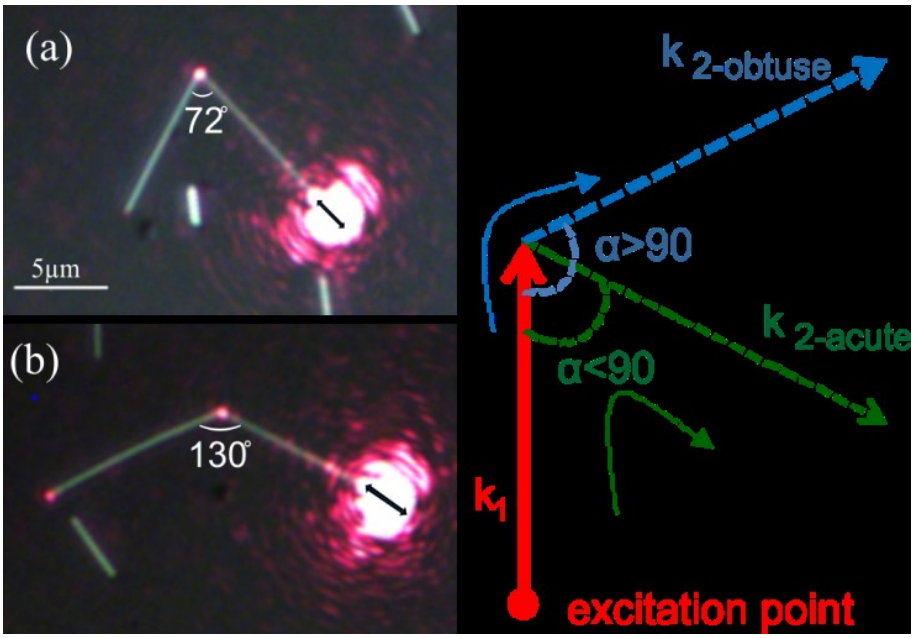

FIGURE 2.7: Optical image of plasmon-assisted light propagation in Ag NW dimer with a bending angle of (a) 72^o and (b) 130^o . Black arrows indicate polarization of incident light at 632.81nm wavelength. (c) Vector representation of plasmon propagation in acute and obtuse angled wire.

the distal end of the Ag NW dimer, with scattering losses at the NW junction. These angle-dependent light emissions can be understood by simple geometrical arguments as follows: Consider the k vector of plasmon propagation in Ag NW dimer as shown in Figure2.7c. The excitation of plasmon polariton at one end of Ag NW dimer (red dot in Figure2.7c) leads to SPP propagation as shown by the k1 vector (red arrow). Now there are two scenarios for the k1 vector to propagate depending upon the bending angle between the Ag NWs: one is that if the angle between the Ag NWs in acute ($\alpha <$ 90), the k1 vector scatters at the nanowire junction leading to light emission and further propagates as vector k2-acute along the second nanowire (green dashed line).

As one may observe, there is a large curvature in the acute angle scenario, leading to a greater bending loss and hence very weak emission at the distal end of the Ag NW dimer (see Figure2.7a). On the other hand, when the bending angle between the Ag NWs is obtuse ($\alpha >$ 90), the k1 vector scatters off the junction and further propagates as vector k2-obtuse as shown in Figure2.7c (blue dashed arrow). Note that the curvature for the obtuse angle scenario is less leading to lesser bending loss and hence greater intensity of light is observed at the distal end of the Ag NW dimer (see Figure2.7b). Similar observations were made in a variety of acute- and obtuse-angled Ag NW dimer shown in Figure2.8. Images in Figure2.8 show the light emission at junction and distal ends of Ag NW dimers for acute angles (a and b) and obtuse angles (c and d) between Ag NWs. It was evident that obtuse angled wires lead to better transmission. We

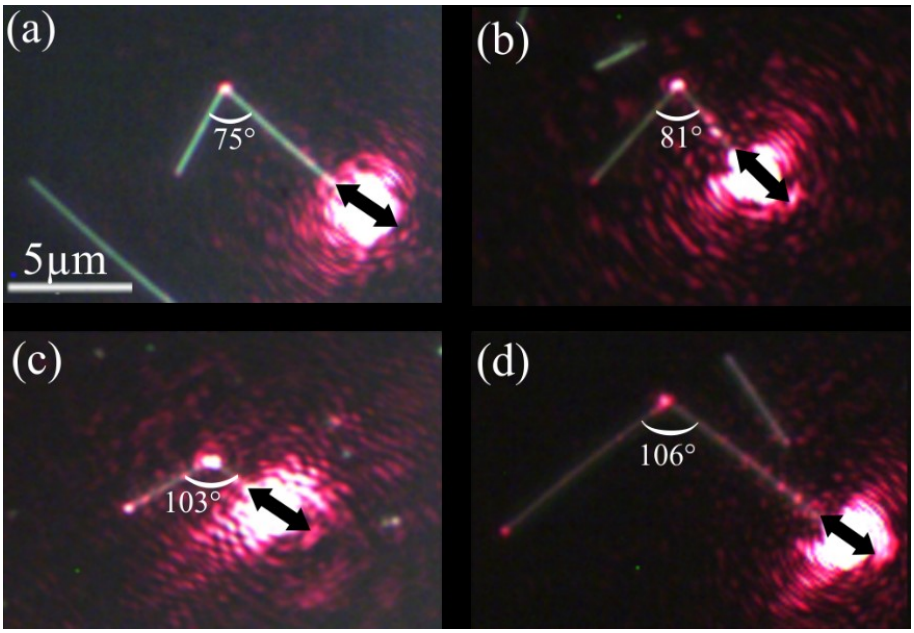

FIGURE 2.8: Light propagation through different angular Ag NW dimer. Black arrow shows the polarization of incident light. (a) Optical image of Ag NW dimer with 75^o angle (b) optical image of Ag NW dimer with 81^o angle; (c) optical image of Ag NW dimer with angle of 103^o; (d) optical image of Ag NW dimer with angle of 106^o

emphasize that such subtle difference in the angle between the Ag NWs plays a critical role in the SPP-mediated transmission characteristics, and hence should be taken into consideration during the design of SPP-based circuits.

2.3.3 Polarization dependent light propagation in serially couple Ag NWs

With the hindsight that obtuse-angled nanowires exhibit better propagation of light, we probed the light emission characteristics in obtuse-angled Ag NW dimers as a function of polarization of incident light. In Figure2.9a and b we have shown polarization-controlled light emission at the junction and distal end of Ag NW pair. When the polarization of incident beam was along the direction of the input Ag NW, we observed light emission at the junction and distal ends of the Ag NW dimers, which represents ON state. When the polarization was oriented perpendicular to the length of the input Ag NW, no light was observed at the junction and distal ends of Ag NW dimer, representing an OFF state. Furthermore, when the input polarization direction was in between parallel and perpendicular to the Ag NW length, we observed systematic $\cos^2\theta$ dependence in the intensity of emitted light at the junction and distal ends of Ag NW dimers (see polar plot in Figure2.9c). The physical origin of this observation is as follows:

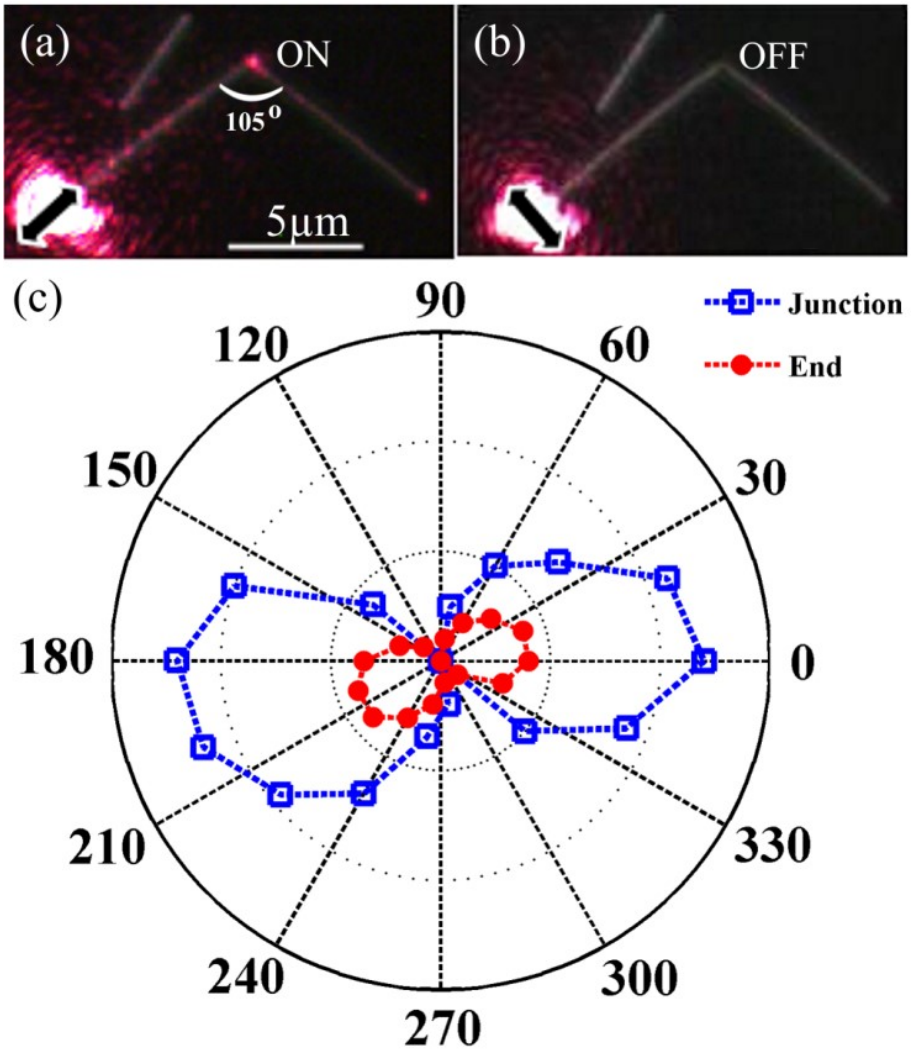

FIGURE 2.9: Polarization controlled emission from Ag NW dimer. (a) Optical image of the ON state: light is emitted at the junction and distal end of Ag NW dimer; (b) corresponding OFF state: no light emitted at the junction and distal end of Ag NW dimer. The black arrows indicate the direction of electric field polarization, (c) Polar plot indicating input polarization tuned light emission from the junction (square, blue) and distal end (round, red) of Ag NW dimer.

for the given cylindrical geometry of the Ag NW, there are two allowed modes [126, 128]: $m = 0$ and $m = 1$. The $m = 0$ mode is represented by electric field along the length of the nanowire, and $m = 1$ mode is represented by electric field perpendicular to the length of the wire. The $m = 0$ mode, results in the light emission at the distal end, whereas $m = 1$ mode does not result in emission of light. Figure2.1 confirms this particular concept with experiments and finite element methods simulations on single Ag NW. In the context of Ag NW dimer, this indicates that when the polarization of light is along the length of input nanowire, the $m = 0$ mode is excited, and a major

part of the plasmon polaritons are converted into free photons at the junction leading to the ON state (Figure2.9a). Interestingly, a small fraction of the plasmon polaritons does tunnel into the second nanowire, further leading to emission of light at the distal end. In the OFF state (Figure2.9b), the input polarization is perpendicular to the length of the nanowire ($m = 1$ mode). This configuration does not facilitate light emission either at the junction or at the distal end of the Ag NW dimer.

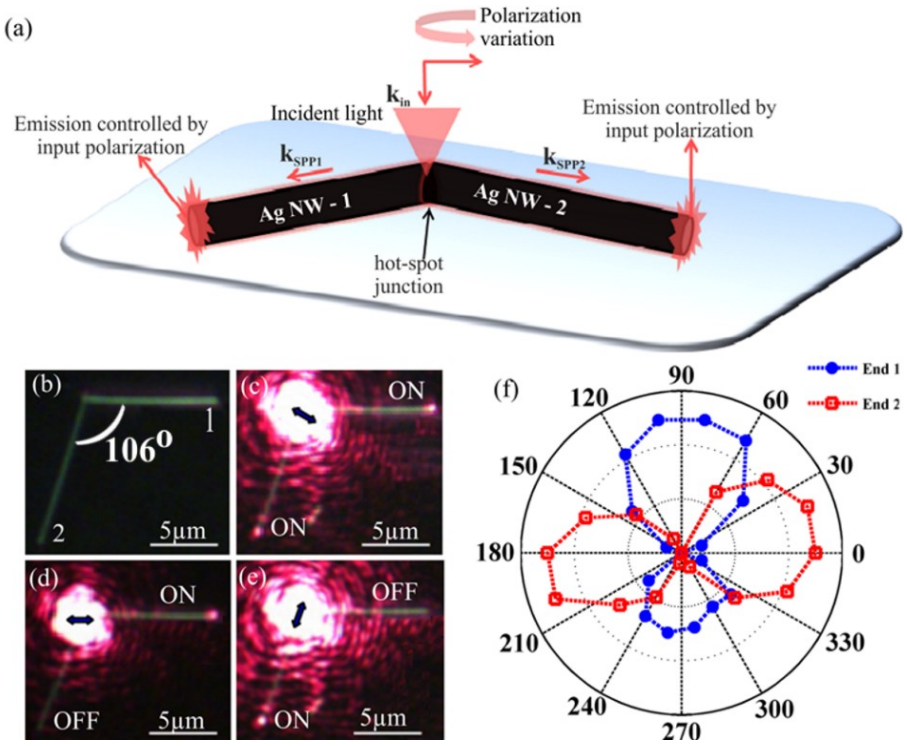

FIGURE 2.10: (a) Schematic of the experimental configuration to show plasmon routing capability of Ag NW dimer. (b) Optical image of Ag NW dimer used for the study; (c) shows the emission of light at the both ends of Ag NW; (d) end 1 is in ON state and end 2 is in OFF state; (e) end 2 is in ON state and end 1 is in OFF state; (f) Polar plot indicating the input polarization controlled plasmon routing at the end 1 (circle, blue) and 2 (square, red).

For any other polarization angle, the excitation is a combination of $m = 0$ and $m = 1$ mode leading to systematic variation in the intensity of the emitted light at the junction and distal end of Ag NW pair. These observations clearly indicate that by varying the input polarization of light at one end of the Ag NW dimer, one can control the light emitted at the junction and distal ends. Such remote excitation and control of emission of plasmonic nano-junction can have implications in scenarios where there is a necessity to create spatial off-set between the input excitation and output emission channels in plasmonic circuitry, thus avoiding effects of interference.

Can this polarization dependence be used to route light in Ag NW dimers? To answer this question we further tested our Ag NW dimers for light routing capability of obtuse-angled Ag NW dimer. The excitation configuration was different as compared to Figure2.6. In Figure2.10a we show the experimental schematic to test the light routing capability in Ag NW dimer. The location of illumination was at the Ag NW junction; and by varying the polarization of the incident light at the NW junction, we observed the emission of light at two ends of the Ag NW. Figure2.10b shows the optical image of Ag NW dimer. In Figure2.10c we observed emission at both ends of the Ag NW when the polarization of the incident beam had a projection on both of the nanowire axis. However, when the polarization was oriented such that the electric field was along one of the axes of nanowires (see Figure2.10d and e); we observed emission of light from only one end of the Ag NW dimer. In polar plot shown in Figure2.10f, we show the variation of emitted light intensity at the two ends of the Ag NW dimer as a function of input polarization at the Ag NW dimer junction.
Clearly, we observed that the emission patterns at two ends of Ag NW dimer are complementary to each other. The above-discussed data implies that by varying the incident electric field polarization at the nano-junction of Ag NW dimer, the plasmons could be routed along the desired path. It is to be noted that the plasmon routing capability in our work has been achieved without changing the location of the illumination, and hence such optical configurations can find applications in on-chip plasmonics where it is desirable to have a minimum number of illumination channel with multiple emission ports.
Another important issue in nanophotonic circuitry is the polarization beam splitting of light at subwavelength scale [117]. We performed experiments to test the output polarization of the light emitted at the nanowire junction and distal ends and possibility of polarization beam-splitting. The experiment was performed in two excitation configurations (distal and junction excitation) and three polarization collection configuration (no analyzer, vertical analyzer, and horizontal analyzer) as shown in Figure2.11. Figure2.11a shows the optical image in which incident light was polarized (indicated by black arrow) and the collected images were not filtered with any polarization analyzer.

This configuration resulted in bright emission at the junction and distal ends of Ag NW dimer. In the next case (Figure2.11b), the excitation polarization was same as in Figure2.11a, but we introduced a vertical polarization analyzer before the CCD camera. The white arrow in Figure2.11b shows the direction of polarization of the emitted light. This configuration resulted in brighter emission at junction and a very weak emission at the distal end, indicating that the majority of the photons emitted at the junction were vertically polarized. For the next case (Figure2.11c), we turned the polarization analyzer to horizontal direction (see white arrow in Figure2.11c), and observed

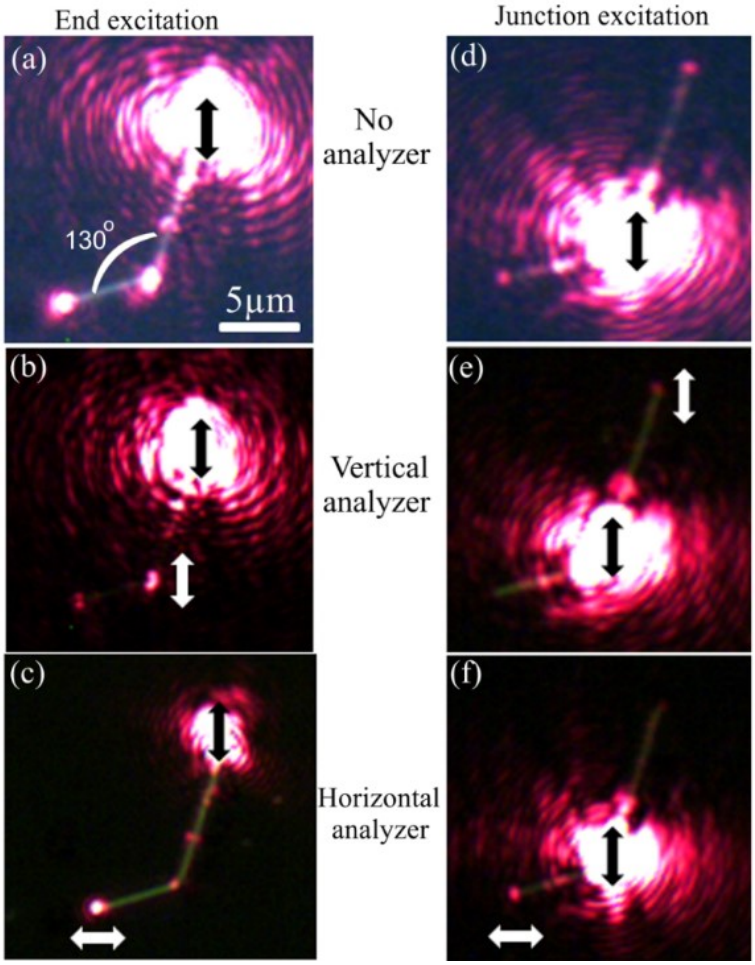

FIGURE 2.11: Optical images of Ag NW dimer emitting polarized light. The left and the right columns indicate two different configurations of excitation. The left panel shows excitation channel at one of the Ag NW dimer and emission at the junction and distal ends; (a) without analyzer, (b) with vertical analyzer and (c) with horizontal analyzer. The configuration of right panel is similar to the left except that the excitation is at the junction of the Ag NWs. In all the images, the black arrow indicates input polarization and the white arrow indicates output polarization. Images (e) and (f) indicate polarization beam splitting of Ag NW dimmers.

brighter emission at the distal end and a very weak emission at the Ag NW junction, indicating that the majority of the photons emitted at the distal end were horizontally polarized. Next, we repeated these experiments by illuminating the Ag NW dimers at the junction (Figure2.11d-f). The most interesting observation was that by illuminating Ag NW dimers at the junction, one could use this configuration as polarization beam splitter (compare Figure2.11e and f). We observed that each arm of the Ag NW dimer facilitated complementary paths for light emission with respect to output polarization, thus showing the capability of Ag NW dimer as a polarization beam splitter at subwavelength scale. The above experiments show the versatility of Ag NW dimer configuration

with respect to input and output parameters of light and can be further harnessed as a nanophotonic circuit element.

2.4 Conclusion

To summarize, we have shown that angle between the self-assembled Ag NW dimer plays a critical role in light propagation. The polarization of incident light can be harnessed to control the emission at the junction and distal end of Ag NW dimer. Such nano-plasmonic configurations can be employed as plasmonic circuit elements for on-chip nanophotonics and plasmon resonance tunnelling [129]. In the current study, we used single excitation wavelength (632.81 nm) to create plasmons. By employing multiple excitation wavelengths, our geometry can be extrapolated to realize multicolour light routing. By further tailoring our design, one could include multiple channels for plasmonic routing, where the distal end of Ag NW can be further utilized as nanoscale light sources. Thus, we have shown that Ag NW dimer structures can indeed be an extremely versatile geometry for nanophotonics, and we envisage that many other interesting concepts can be derived from this simple, yet effect design at nanoscale.

Chapter 3

Directional Out-Coupling of Light From a Plasmonic Nanowire-Nanoparticle Junction

Chapter 3 is an adaptation of the research article '*OPTICS LETTERS, 40(6), 1006-1009, 2015*'. The article describes the directional out-coupling of light from a plasmonic nanowire-nanoparticle (NW-NP) junction.

3.1 Introduction

The ability to control and direct light at nanoscale is an important challenge in nano-optics and nanophotonics. To achieve this, plasmons, which are collective oscillations of light and free-electrons at a metal-dielectric interface, have been employed for sub-wavelength propagation and localization of light [130]. Plasmons can reduce the mismatch between the cross-section of an excitation optical beam and absorption cross-section of emitters such as atoms, molecules, and quantum dots, thus mediating and enhancing light-matter interaction [131]. A variety of plasmonic geometries has been innovated and studied in the context of enhancing light-matter interactions. One such geometry is chemically-prepared silver nanowires (Ag NWs) [132–135]. These Ag NWs have atomically smooth surface that facilitates sub-wavelength propagation of surface plasmon polaritons (SPPs) over a distance of a few microns [136]. They can be used as plasmonic resonators [137], logic gates [138], spontaneous emission amplifiers [139], single photon sources [140–142], photon-to-plasmon convertors [143], and have opened up new opportunities in quantum plasmonic circuits [144] and nanoscale quantum optics [145].

In the context of NW-based SPP waveguiding, one of the issues to be addressed is to deterministically convert propagating SPPs into directional photons at a desired location on the nanowire. Such directional out-coupling of light from propagating SPPs of

NW can be further utilized to influence enhancement and directionality of spontaneous emission from emitter in the close vicinity.

Motivated by this requirement, herein we experimentally show how an Ag nanoparticle (NP) in close proximity to Ag NW can out-couple light in a directional manner, thereby acting as a nanoscale optical antenna. One of the important observations we make is that the NW-NP junction can out-couple photons in single and dual directions and further influence directionality of fluorescence emission from molecules in close proximity to NW-NP junction.

3.2 Experimental Section

3.2.1 Synthesis and sample preparation

Synthesis

The nanowire –nanoparticles system were synthesized using wet chemical process, seed-mediated polyol process. Initially, the nanowires synthesis were done using following process: the two solutions A and B were prepared separately where A is 0.085M $AgNO_3$ in 3ml EG (EG: ethylene glycol) and B is 0.340M PVP in 3ml EG, respectively. These two solutions were injected in the preheated at 160 degree 5ml of EG at the rate of 0.2ml/min. Here, the rate plays a crucial role in the formation of nanowire geometry. The slow rate can produce the thicker wire whereas fast injection rate can give thinner wires. We have optimized the injection rate for the wire geometry which essentially produces 150nm to 200nm diameter. After injection, the entire two solutions, the whole suspension was left for one and half hour for stirring at the 160 degree centigrade temperature. Now the entire nanowire suspension was cooled and centrifuged to remove PVP and EG. The solvent of nanowire suspension was kept ethanol because it helps to prepare sample for the experiments.

Sample preparation

The sample for an optical measurement was prepared in following way. The suspension was drop cast on the cleaned glass cover slip (dimension (mm): 25X60X0.17). The suspension contains silver nanowires and nanoparticles. Suspension was diluted in such a way that the nanowires were got well dispersed on the cover slip. The dilution of suspension is important here because it prevents the formation of aggregates on glass cover slip. The nanowire nanoparticles system were formed by the self-assembled process and we have found them using an optical microscope. The experiment of Rayleigh

light scattering from the nanowire-nanoparticle system were performed using pristine nanowire-nanoparticle system. On the other hand, we have also performed experiments for directional fluorescence experiment from the same system. For this experiments, the given nanostructure system was coated by Nile blue molecule with PVA polymer matrix. PVA polymer was coated using spin coating method. The entire nanostructure system was arrested in the polymer matrix where Nile molecules were present in the vicinity of nanowire-nanoparticle junction.

3.2.2 Nanowire-nanoparticle system

The nanowire-nanoparticle system was characterized using various imaging tools such as optical microscopy system and field emission scanning electron microscopy system (FESEM). The morphology of NW-NP system was correlated between optical microscope and FESEM microscopy system. Figure3.1a shows the optical bright field image. Figure3.1b and c presents the same wire with higher spatial resolution which was captured through the FESEM microscopy system. the The correlation between these two microscopy system was done with the help of grid slides where we can mark the location of the nanostructures.

3.2.3 Experimental configuration

The following schematic shows the optical experimental configuration of the basic principle behind the process of directional light emission from Ag NW-NP junction.

Figure3.2a shows the schematic (top view) of the geometry under study. It consists of an individual Ag NP which is in contact with an Ag NW. Both NW and NP are resting on a glass coverslip. The SPPs waves on the NW can be optically excited by focusing a laser beam at two distal ends of the NW (Figure3.2b). Such excitation can be achieved by focusing the laser beam either through the glass substrate (excitation e1 leading to SPP with wave vector k1 in Figure3.2b) or through the air medium (excitation e2, wave vector k2 in Figure3.2b). These excitations can be operated sequentially or simultaneously. The SPPs propagate along the length of the nanowire with a momentum greater than the free space wavelength used for excitation [146]. Therefore, to convert SPPs back to photons at a desired location of NW, momentum has to be subtracted from the surface-bound SPP waves. The Ag NP in contact with the Ag NW acts as a defect center to overcome this momentum mismatch and facilitates the conversion of SPPs to free-space photons at NW-NP junction.

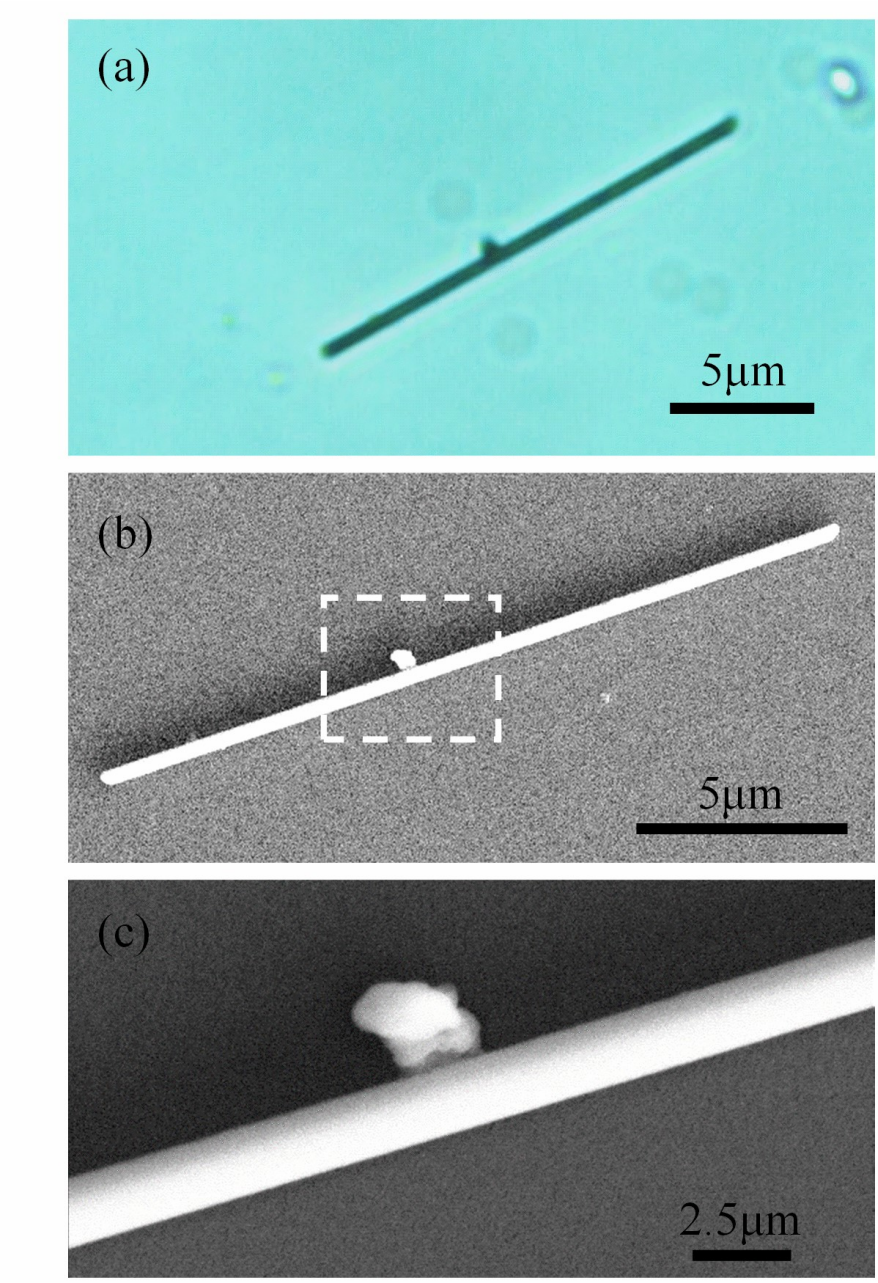

FIGURE 3.1: The nanowire –nanoparticle system were characterized using optical microscopy and FESEM system. (a) Shows the optical image of NW-NP system. (b) Shows the FESEM image of same NW-NP system shown in (a). (c) Indicates the junction (shown in white dashed rectangle in (b)) which were captured at a higher resolution to visualize more clearly about the particle position at the surface of NW.

3.2.4 Optical setup and nanowire-nanoparticle system

One of the aspects of this conversion mechanism is that the scattered light from NW-NP junction is directional in nature, and the directionality of the light can be measured using far-field optical microscopy. Figure3.3a and b show a representative scanning

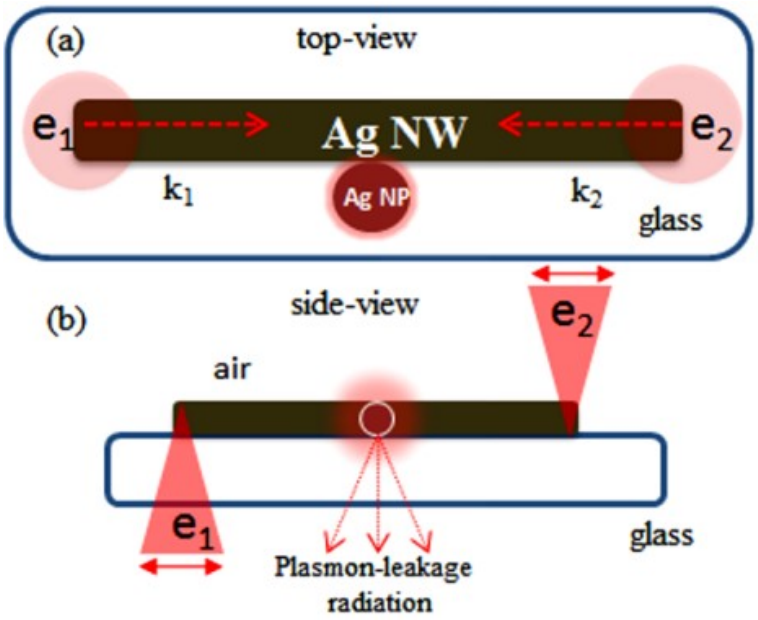

FIGURE 3.2: (a) Schematic of the top-view of the experimental configuration of Ag nanowire (NW) coupled to a single Ag nanoparticle (NP), both placed on a glass coverslip. The regions e1 and e2 are two focused laser excitations at 633nm that launch SPPs. The double-sided arrows indicate the polarization of excitation.

electron microscopy (SEM) image of NW-NP system resting on a glass substrate at two different magnifications. It can be observed that the NW and NP are in contact with each other (Figure3.3b). Such NW-NP systems can be consistently synthesized (see Figure3.3c and d for another NW-NP sample) using polyol method [147] and details of preparation can be found elsewhere [148]. The region of interest for our study is shown as dashed square box in Figure3.3a and c. This is the NW-NP junction from where the optical signals were spatially filtered and collected using a home-built two-channel optical microscope (Figure3.3e). This microscope had the capability to (i) excite distal ends of the Ag NW either through the glass substrate (lens1) or through the air medium (lens 2) by focusing 633nm laser light; (ii) spatially filter light from the desired location along the length of the NW (pinhole in Figure3.3e); (iv) capture real- and Fourier-space optical images (L2, L3, CAM in Figure3.3e) from spatially filtered region and (iii) record Fluorescence spectra and image from the desired location (spectrometer in Figure3.3e). The inset of Figure3.3e shows an optical image of an NW-NP sample excited at two distal ends. The dashed circle in the inset figure shows the out-coupled light from the NW-NP junction.

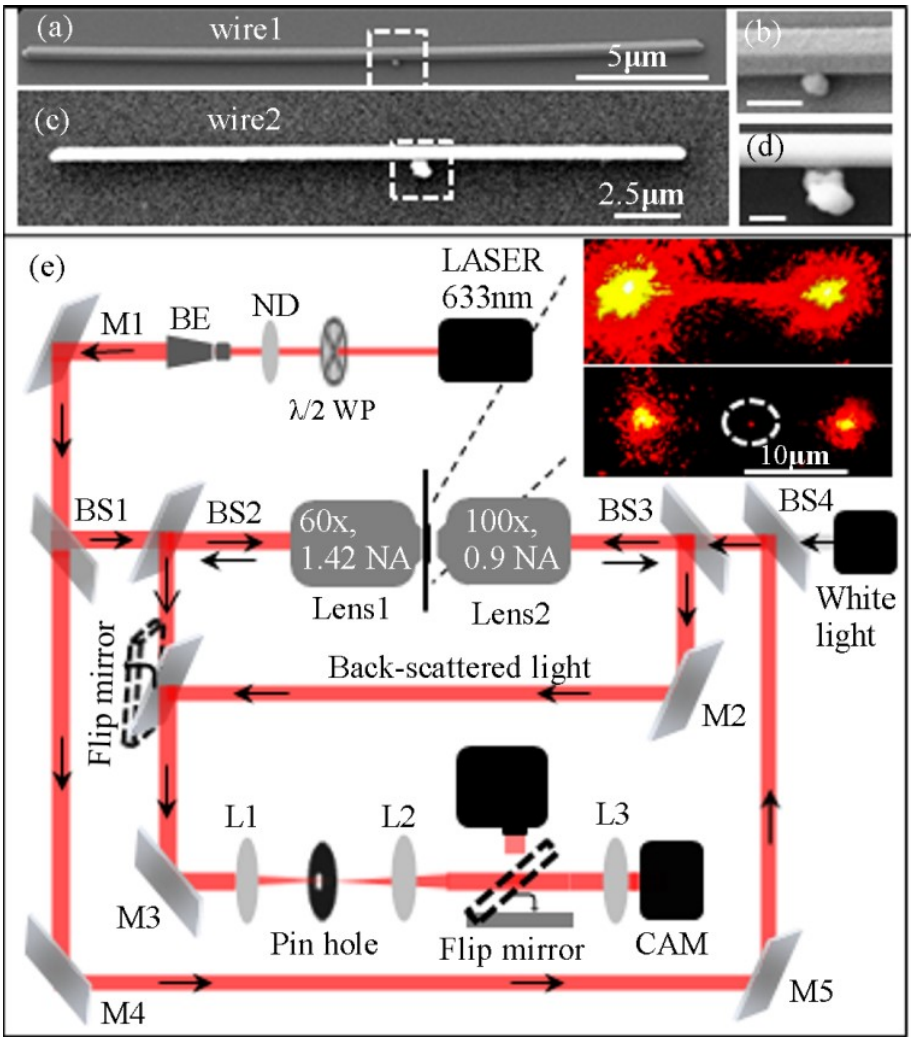

FIGURE 3.3: Scanning electron microscopy (SEM) image of NW-NP system resting on glass coverslip at (a) lower magnification with the dashed region showing (b) NW-NP junction (scale bar 200 nm). SEM image of a different NW-NP system imaged at (c) lower and (d) higher magnifications. (e) Schematic of the dual-channel Fourier microscope with spatially filtered collection. M1, M2, M3, M4, and M5 are mirrors; BS1, BS2, BS3 and BS4 are beam splitters; L1, L2 and L3 are lenses; BE-beam expander; ND-neutral density filter; WP -half wave plate; S is sample stage; lens1 is oil immersion objective lens and lens2 is an air objective lens. Upper and lower insets show an optical image of pristine Ag NW and an Ag NW-NP system excited (633nm) at two distal ends. The dashed circle shows the light emanating from NW-NP junction.

3.3 Optical measurements

3.3.1 Directional emission of Rayleigh light from the NW-NP junction

We studied the directional characteristics of emission of light from the junction with three excitation configurations. The excitation configurations include, the NW-NP system were excited one end at a time and the emission from the junction were recorded accordingly. After excitation both the ends one by one, both ends were also excited simultaneously and again the emission from the junction were captured. The details of this configuration are described in the following sections.

Configuration 1

Figure3.4a shows the optical image of an NW-NP system excited through the glass. The polarization of the excitation source was along the length of the NW as shown by the arrow in Figure3.4a. The dashed circle indicates out-coupled light from NW-NP junction. This spatially filtered region was further imaged in Fourier plane (Figure3.4b) of high NA objective lens (1.42NA, 60X). The angular distribution of intensity in the Fourier plane is given by I (ϕ, $n.\sin(\theta)$), where tangential angle ϕ varies from 0 to 2π and the radial angle $n.\sin(\theta)$) is the numerical aperture of the lens2 with n presenting the refractive index. The inner circle in the image Figure3.4b is of radius 1, indicating the critical angle at glass-air interface, and the outer circle is of radius 1.42 indicating the maximum aperture radius.

The NW axis is considered as x direction, and k_x, k_y represent the wavevectors along x and y-direction, and k_0 represents the wavevector of the free photons (k_0= $\frac{2\pi}{\lambda}$, where λ is the free space wavelength of excitation).Two features were evident in the Fourier-plane image (Figure3.4b). The first feature was a straight line for a constant value of $\frac{k_x}{k_0}$, and the second was an arc-like feature close to periphery of the outer circle. The straight line indicated the guided mode of the SPP propagating along the length of the NW [146], and the arc indicates the directional light scattered from the NW-NP junction. Such directional light scattering has been previously observed only from the distal ends of the NW [149]. Here we have shown, for the first time, directional light emission from a plasmonic NW-NP junction.The arc in Fourier plane was further quantified to determine the spread in the directionality (Figure3.4c), and we found the value to be of 21 degrees.

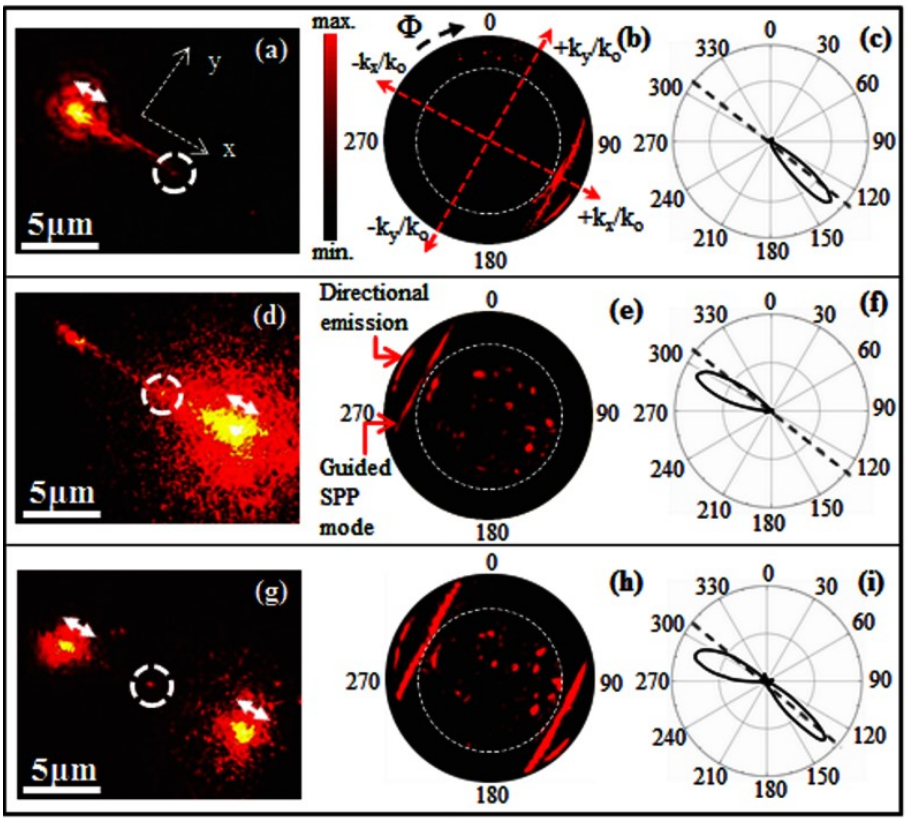

FIGURE 3.4: (a) Real-space optical image of Ag NW-NP junction (Figure3.3a) remotely excited according to e1 excitation in Figure3.2. The NW is along x-axis. White dashed circle shows the light from NW-NP junction. (b) Fourier-plane ($\frac{k_x}{k_0}$, $\frac{k_y}{k_0}$) intensity (I) image of light from NW-NP junction. The tangential angle is given by ϕ and the radial angle is given by NA of the lens. The inner dashed circle indicates the critical angle at glass-air interface. (c) I Vs ϕ for the arc-emission from NW-NP junction for e1 excitation configuration. (d) Real space image for e2 configuration and corresponding (e) Fourier space optical image from NW-NP junction and (f) I Vs ϕ plot. (g) Real space image for e1+e2 configuration and corresponding (h) Fourier space optical image from NW-NP junction and (i) I Vs ϕ plot. White arrows indicate polarization axis of excitation and dashed lines indicate NW orientation.

Configuration 2

Figure3.4d shows the optical image of an NW-NP system excited through the air medium. Similar to the previous case, we found that the Fourier plane image showed the guided SPP mode and an arc indicating directional light emission (Figure3.4e). We further quantified the directionality of the emission (Figure3.4f) and found a spread of 24 degrees.

Configuration 3

Next, we simultaneously excited the distal ends of the Ag NW via glass and air medium (as shown in the optical image of Figure3.4g) and captured the light emerging from the NW-NP junction and projected it to the Fourier plane (Figure3.4h). We observed two guided modes and two arcs towards the periphery of the outer circles. The two arcs of light essentially indicated dual channel scattering and are the central finding of this chapter. The directionality of the dual channel was further quantified (Figure3.4i) and the feature of the emission was found to be a sum of the features observed in Figure3.4c and f. All the data in Figure3.4 implied that the NW-NP sub-wavelength junction functioned as a single and dual channel directional scattering point. It is to be noted that parameters such as NW-NP distance, the shape of NP and NW morphology can also influence the directionality. This motivates further studies on such NW-NP systems.

3.3.2 Directional emission of fluorescence light from the NW-NP junction

In principle, SPPs in NW couple to NPs leading to directional scattering. Such directional scattering can be further used to excite molecules. Can the NW-NP junction influence the directionality of the fluorescence from emitters? To answer this question, we extrapolated our geometry to the configuration shown in Figure3.5a. A nano-film (50 nm thickness) of PVA doped with fluorescent molecules (Nile blue A) was spin-coated over the NW-NP system. Then, we illuminated the ends of the Ag NW through glass substrate and captured the plasmon-coupled fluorescence emission from NW-NP junction.

The fluorescence spectra from the NW-NP junction is displayed in Figure3.5b with the inset showing the fluorescence image captured from the geometry. The dashed circle in the inset figure shows the fluorescence emission from the NW-NP junction. This fluorescent light was further projected to the Fourier-plane of a high NA lens (as discussed previously) to determine the directionality of the emission. Figure3.5c shows the Fourier-space image for e1 illumination. We found that the fluorescent light collected from the NW-NP junction was indeed directional in nature. We further quantified the directivity of emission and the spread in the angle ϕ was found to be 46 degrees (Figure3.5d). The dashed line in Figure3.5d indicates the orientation of the long axis of the NW. Figure3.5e shows fluorescence emission in Fourier-plane when the another end of NW was illuminated (e2 illumination). We found that the directionality in the Fourier-plane was almost opposite (Figure3.5e), and the data in Figure3.5f showed a spread in

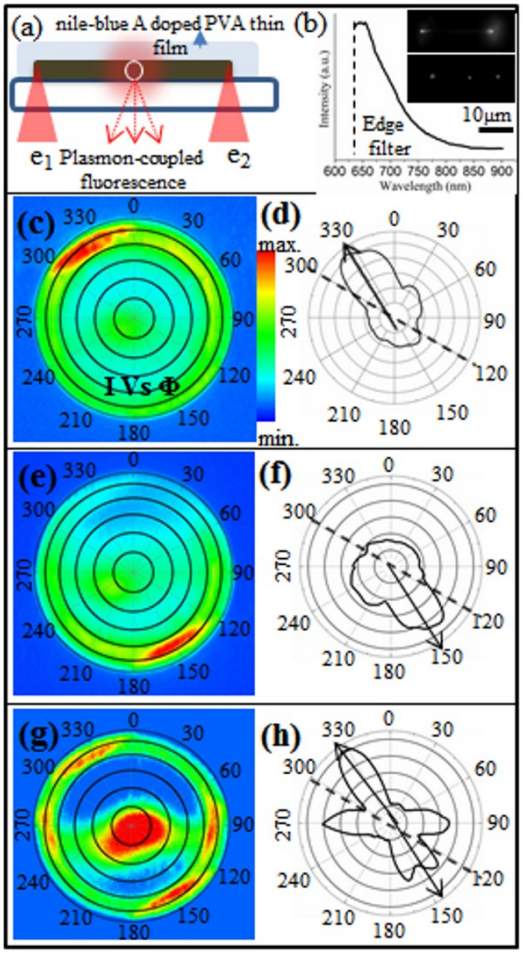

FIGURE 3.5: (a) Schematic of the experimental configuration to probe directional fluorescence emission from NW-NP junction. (b) Fluorescence spectra of the emission from the spatially filtered NW-NP junction, with the upper and lower insets showing fluorescence image of NW (without NP) and NW-NP system, respectively. (c) Fourier-plane optical image from NW-NP junction and (d) I versus plot for e1 excitation. (e) Fourier space optical image from NW-NP junction and (f) I versus plot for e2 configuration. (g) Fourier space optical image from NW-NP junction and (h) I versus plot for counter-propagating e1 + e2 excitation. The dashed black line in polar plots shows the orientation of Ag NW

the angle ϕ to be 54 degrees. Next, we exited the counter-propagating plasmons by exciting both ends of the NW (e1+ e2 illumination), and we recorded the Fourier-space image of the light emerging from NW-NP junction (Figure3.5g). The feature of the emission had two pronounced directions (along 330 and 150 degrees in Figure3.5h). In addition to this, we observed emission along angles 90 and 270 degrees. These emission directionality with geometrical features of the NW-NP junction need further investigation for complete understanding. All the data in Figure3.5 suggests that NW-NP junction can function as single and dual channel optical antenna, which can further

influence the directionality of fluorescence emission.

3.4 Conclusion

To conclude, we have shown Ag NW-NP junction can be utilized as single and dual-channel optical antenna that can influence directivity of elastic scattering and fluorescence emission of molecules. As a future prospect, it would be interesting to place single emitters, such as nitrogen-vacancy in diamond [142], close to the NW-NP junction and explore the single-photon emissivity. As the mode volume of the NW-NP junction is expected to be very small, one should expect the Purcell enhancement factor to be very large at such junctions. Such geometries not only enhance the rate of spontaneous emission from emitters but also influence their directionality.

Chapter 4

Angular Emission from 1D and 2D Meso- and Nano-Structures: Probed by Dual-Channel Fourier-Plane Microscopy

Chapter 4 is an adaptation of the research article *Optics Communications, 398, 112-121 (2017)*. The article describes the angular emission from an organic waveguide resonator and 2D layered material at an dielectric interface which is probed by dual-channel Fourier-plane photoluminescence microscopy system.

4.1 Introduction

Controlling the directionality of light emanating from a sub-wavelength structure has emerged as an important topic of research in nanophotonics [150–152]. To this end, various nanostructures made of metal [153–157] and semiconductors [158–162] have been studied, and a variety of geometries [163–165] have been proposed and realized. One such variety is a self-assembled, mesoscale, organic molecular waveguide [166–170]. Such quasi-one-dimensional structures facilitate Frenkel exciton-polaritons [171, 172] and Fabry-Perot resonances, and can be harnessed to guide light not only at excitation wavelength but also at the Stokes shifted excitonic emission [173–175]. Due to such capabilities, organic waveguides can be harnessed for various nanophotonic applications including micro-nano-scale laser [176, 177], resonators [178–180], active optical antennas [157, 174, 175] and photonic sensors [170, 181, 182].

Generally, for optical device applications, an organic waveguide resonator is either grown or deposited on a transparent dielectric substrate and optically interrogated using a high-numerical-aperture objective lens housed on a microscope. Such characterization is performed by exciting the waveguide either through the transparent substrate or

through the air-superstrate. As a consequence of solution to Maxwell's equation, it is well known that when a molecule (dipole emitter) is placed at an interface of two dielectric media [183], majority of the emitted light escapes through the dielectric medium of higher refractive index, and some percentage of light escapes into the lower index medium. In addition to this, the angular distribution and spectral feature of the light emitted into substrate and superstrate also differ [183–185]. Therefore, in the context of the organic waveguide, there is an imperative to characterize the emission intensity and angular distribution of the waveguided Frenkel exciton-polariton emission through the substrate and superstrate. Importantly, the contrast in the dielectric constant at the interface can be harnessed to engineer optical emission from organic mesostructures.

4.2 Experimental Methods and Instrumentation

4.2.1 Experimental Methods

In this article, we report on the observation of angle-resolved, waveguided-photoluminescence (PL) emission from an organic mesowire waveguide made of 1, 5-diaminoanthraquinone (DAAQ) molecules into glass-substrate and air-superstrate. For a given organic nanowire, we specifically quantify the polar and azimuthal angle-resolved PL emission through the substrate and superstrate by employing dual-channel Fourier-plane PL micro-spectroscopy. We show that there is a quantitative difference in the emission angle and finesse of Fabry-Perot modes for the two cases, thus highlight the relevance of dual channel measurements. The DAAQ mesowires were synthesized using physical vapor transport method, and the preparation details are given elsewhere [168]. The basic principle behind the experiment is illustrated in the schematic shown in Figure4.1. The Figure4.1 essentially shows the side view of a DAAQ mesowire resting on a glass substrate. The active wave-guiding mode of DAAQ wire is excited at one end using 532nm laser light from either side of the interface: bottom illumination (Figure4.1a) through the glass medium and top illumination (Figure4.1b) from the air-side. The propagated photoluminescence from distal end of the wires was spatially-filtered and collected using same channels of excitation. The objective of the study was to quantitatively compare the angular PL emission and their spectral features between the case shown in Figure4.1a, b and c.

4.2.2 Optical Instrumentation

To realize the experimental configuration given in Figure4.1, we built a two-channel Fourier-plane photoluminescence microscope whose schematic is shown in Figure4.2.

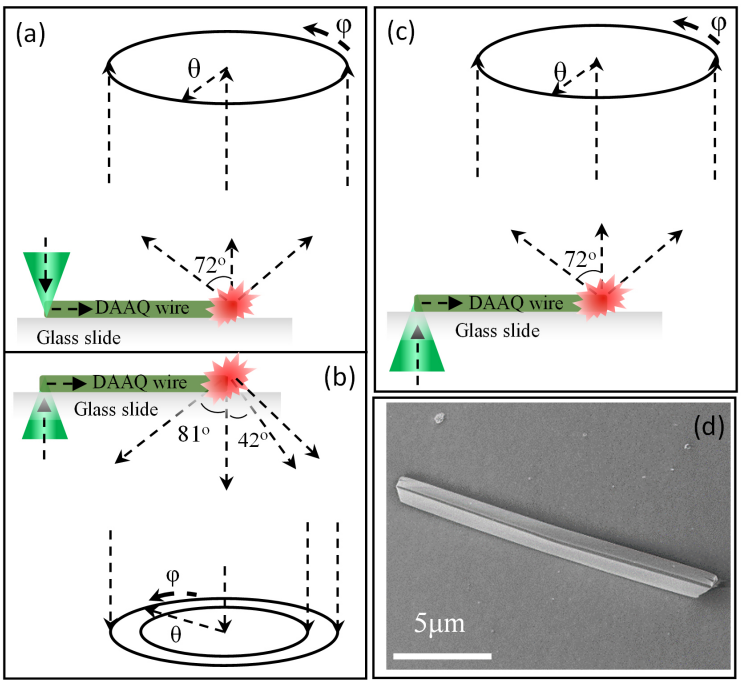

FIGURE 4.1: Experimental configuration of dual channel Fourier plane imaging. DAAQ mesowire resting on an optically transparent substrate (glass coverslip). Excitation and collection of photoluminescence (PL) were performed in three different configurations: (a) From air-superstrate, (b) through the glass-substrate and (c) the transmission mode where the wire was illuminated through the substrate and emitted signals were collected from the top channel (air superstrate). e1 and e2 represent the 532nm wavelength excitation beam focused at an end of wire. (d) Shows the FESEM image of DAAQ mesowire. In the bottom channel, the high NA (1.49) oil-immersion objective lens were used to collect signals. The top channel was equipped with the 0.95NA objective lens. and are spherical coordinates.

The microscope facilitates the excitation and collection of signals from the sample either using lens1 (100x, 0.95 NA) in air medium (superstrate) or through a glass (or transparent) substrate using oil immersion lens2 (100x, 1.49 NA). The lens1 was used to illuminate white light and capture the bright-field optical images through both the channels. The sample was mounted on the XYZ-translation stage which was fixed between two oppositely aligned objective lenses. The incident laser intensity and polarization were controlled by a combination of visible-wavelength half-waveplate (HWP) and linear polarizer (Vis-LP). The laser beam was expanded using beam expanders (BE1 and BE2) to overfill the back aperture of objective lens, which results in tightly focused spot. The collected photoluminescence was filtered out from 532nm pump laser light using 532nm edge-filter (Semrock, BLP01-532R-25).

The collection optics of upper channel and lower channel facilitate the real plane

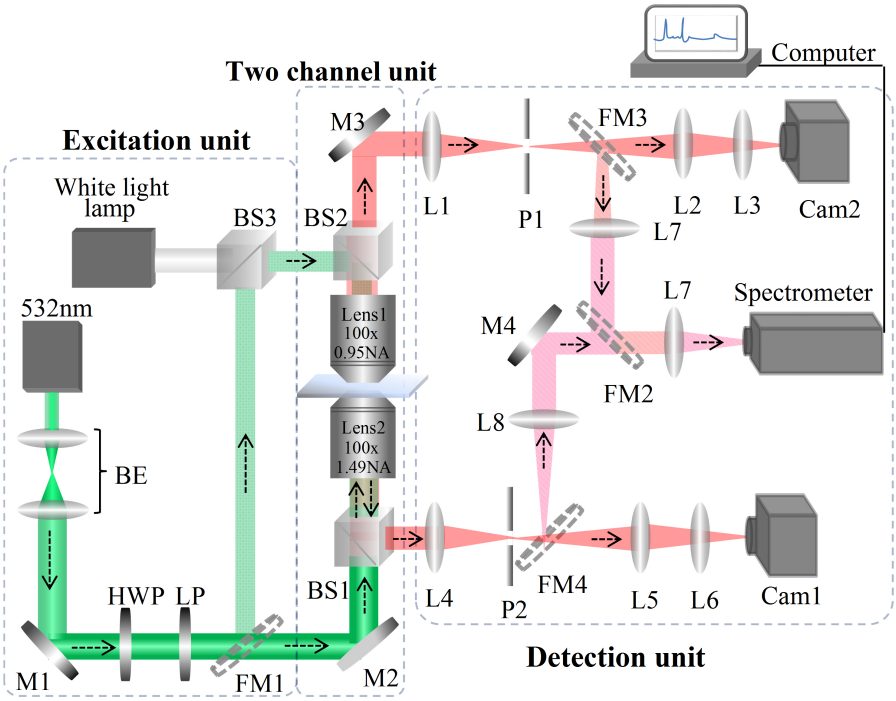

FIGURE 4.2: Schematic of dual channel advanced optical microscopy and spectroscopy system: The entire schematic contains three sections: excitation unit, two channel unit, and detection unit. The excitation unit contains all the illumination sources. The system is equipped with CW laser (532nm) which were routed towards both channels. The laser beams were expanded using telescopes, BE1 (BE: beam expander). Visible Half wave plate (HWP) and visible linear polarizer (LP) were used to control intensity and polarization of the incident light. The two channel unit contains two vertically aligned high numerical aperture, 100x, 1.49 NA and 100x, 0.95 NA, objective lenses (generally called channels). Detection unit facilitates the real plane and Fourier microscopy observation, respectively. Channel includes L1, L2 and L3 are set of lenses which were used to project objective's real plane image and Fourier image on the CCD (Cam2). Similarly, the set of lenses L4, L5 and L6 were used to project the real plane and Fourier plane image on the CCD (Cam1) in channel2. For the spatial filtering of signals, a pin-hole, P1, and P2, were placed at the image plane of L4 and L1, respectively. In addition to the microscopy, a spectrometer was coupled to the common optical path (include signals from both the channels) of light signals for spectral information of light scattering. The silver mirrors M1, M2, M3 and M4; flips mirrors FM1, FM2, FM3 and FM4 were used to route the light and collection of optical signals from both the channels, respectively. BS1, BS2, and BS3 are beam splitters. The White light lamp was used to observe the bright-field optical image of nanostructures. Dotted arrows indicate the direction of propagation of light.

and back focal plane (BFP) imaging (by flipping lens L3 and L6, respectively) systems,

respectively. The two camera (cam1 and cam2) were used for capturing optical images. To record the spectral signature of emission from either of the channels, a spectrometer (Andor, Shamrock) was coupled to the common path of collection optics.

4.3 Results and Discussion

4.3.1 Light propagation and directional emission in the organic DAAQ mesowires:

By using above optical configuration of microscopy and spectroscopy system, the far-field spatial and spectral properties of PL emission from DAAQ measowire were captured through the two media i.e. air superstrate and glass substrate, as shown in Figure4.3 (a) and (b). The Figure4.3(c) shows the PL images of DAAQ mesowire using lower channel optics. The two bright spots at the ends of the DAAQ wire represents the excitation region (big bright spot) and an emission-end of wire (smaller spot). The inset shows the transmission bright field optical image captured through the glass substrate using lower channel lens2. Figure4.3(d) shows the PL image of same DAAQ wire captured using upper channel lens1. The inset shows the back-reflected bright-field optical image of the same DAAQ wire using the upper channel lens1. In order to record the emission signals, the distal end was spatially filtered out using pin-holes P1 and P2 in both channels, respectively. The spatially filtered emission was routed towards collection optics for Fourier plane observation through upper channel and a lower channel, respectively as shown in Figure4.3(e, f). The intensity distribution in the Fourier plane represents the information about angular distribution of emitted signals (photoluminescence) in the coordinate system of θ and ϕ. The far-field intensity angular distribution in the Fourier plane is given by I(θ, ϕ). Here, θ represents the polar angle, which is limited by the numerical aperture of the objective lens. The angle ϕ is the azimuthal angle which varies from 0 to 2π. The Fourier planes of Figure4.3(e, f) contain the inner circle of radius 1, indicating the critical angle of the glass-air interface. The outer radius is 1.49 in Figure4.3(e) indicates maximum aperture radius of lens2 and 0.95 in Figure4.3(f) indicates the maximum aperture radius for lens1, respectively. The long axis of DAAQ mesowire was considered as x-direction. The spectral feature from the two channels is shown in Figure4.3(g) and (h).

In our experiments, we have observed significant differences in the azimuthal spread between top and bottom channel collection. These values essentially indicate the intensity spread in polar-coordinates and may arise due to following reasons :

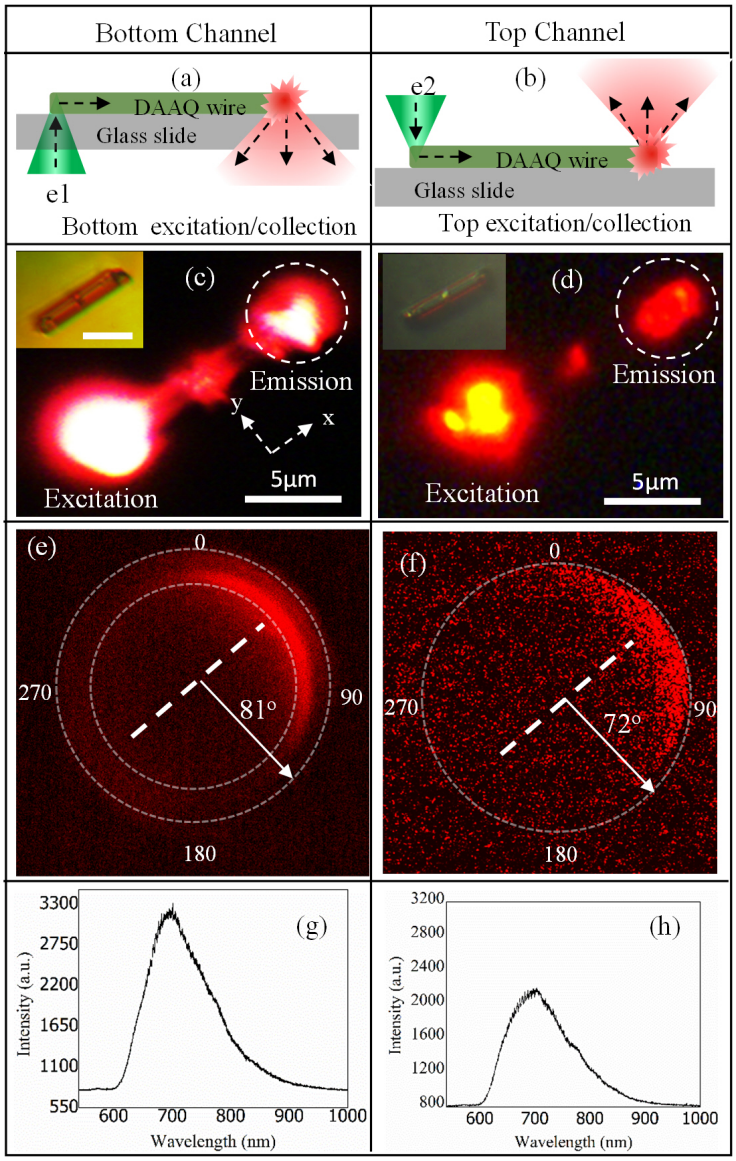

FIGURE 4.3: The excitation of Frankel-exciton polariton in DAAQ mesowire and collection of PL emission were performed in two different configurations: (a) through the glass substrate and (b) from the superstrate. The PL images of a DAAQ mesowire captured from (c) bottom channel and (d) top channels. The insets show the bright field optical images of DAAQ wire captured from the respective channels. Fourier plane PL images from spatially filtered distal ends in the (e) bottom and (f) top optical channels. The respective PL spectra are shown in (g) and (h). The dotted lines in the Fourier plane image indicate orientation of the long-axis of the wire. The white arrows in the Fourier plane image indicate the maximum aperture angle value of collection lens.

1 The geometry of the end morphology has an implication on the emission directionality. In the context of DAAQ mesowires, it has been previously shown [[176]] that morphology at the ends does have a bearing on the azimuthal spread.

What our results indicate, for the first time, is that the azimuthal spread of emission varies not only from one end-morphology to other, but also on the local orientation of the end with respect to an interface. This data further indicates the emission directionality has to be evaluated carefully with respect to the local geometry of the end-morphology of the mesowire and its orientation with respect to an interface.

2. The azimuthal spread in emission may also vary to the local variation in refractive index at the interface. This has been shown in the context of plasmonic silver nanowires, and may be applicable to the organic meso/nanowires.

4.3.2 Quantitative analysis of the angular distribution of photoluminescence in Fourier space

As mentioned earlier, one of the objectives of the study was to quantitatively analyze and compare the angular emission patterns shown in Figure4.3c and d. Figure4.4a shows the variation of intensity of PL emission as a function of θ (see white, dotted line in the inset), for the lower channel Fourier plane measurement. From the plot, the intensity peaked at a radial angle of 46.5 degrees and the measured full width at half maximum (FWHM) $\delta\theta$ was approximately 23 degrees. Figure4.4b and inset show the relevant data for the upper channel emission. In this case, the intensity peaked around 51 degrees and the FWHM $\delta\theta$ was 33 degrees, which was greater compared to the case of lower channel emission. Figure4.4c is a polar plot showing the azimuthal (ϕ) distribution of PL intensity (collected through the lower channel, at θ = 46). The spread $\delta\phi$ was found to be 70 degrees. Similarly, Figure4.4d shows the azimuthal distribution of PL intensity (collected through the top channel, at $\theta = 52$ degree). The spread $\delta\phi$ was found to be 90 degrees. An important inference that we can draw from the above analysis is that the radial and azimuthal angular spread of PL emission into the superstrate were greater than the emission into the substrate and our measurements quantify this difference. The physical reason for such difference in emission angle is due to the fact that whenever molecular dipole emission occurs at a dielectric interface [186], the intensity of emitted light is pronounced towards the medium of higher dielectric (in our case glass substrate).

Furthermore, the angular distribution is sharper at well-defined angles for substrate emission as compared to supersaturate emission. Such differences in emission at dielectric interface has important consequence on emission engineering of exciton-polaritons, where by tailoring the refractive index of the substrate and superstrate, one can vary the angular emission parameters. Such capability of emission engineering may have a direct

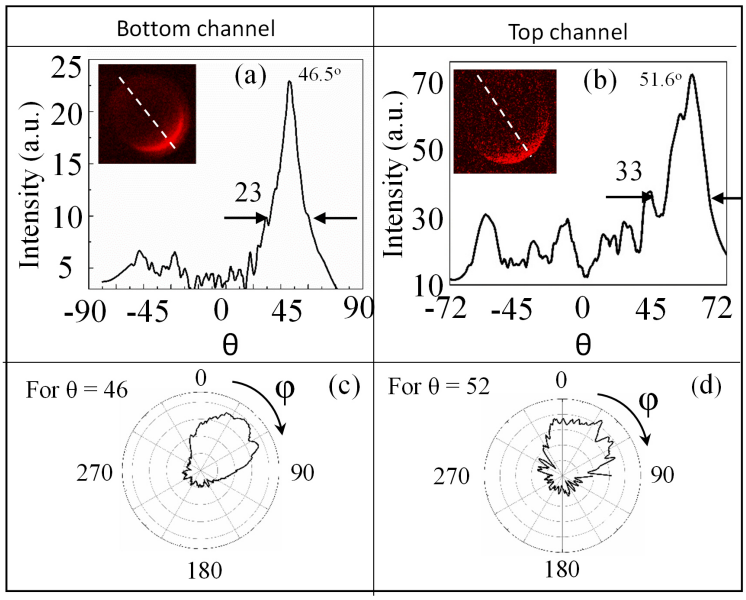

FIGURE 4.4: Quantitative analysis of Fourier plane images captured from bottom and top channels. PL Intensity as a function of radial angle θ for (a) bottom and (b) top channels. The line in the insets shows evaluated θ values. The PL intensity as a function of azimuthal angle ϕ from (a) bottom and (b) top optical channels at the mentioned θ values.

consequence on design of polariton lasers [180, 187, 188] and can be further harnessed for various organic light emitting devices [189–192].

4.3.3 Photoluminescence directional emission in transmission mode

By employing the dual channel microscopy and spectroscopy system, the directional emission characteristics were observed using transmission mode, as illustrated in Figure4.5(a). Such configuration of microscope includes the illumination through the bottom channel and emission were collected from the top channel. The experiment in transmission mode was performed on the same wire which was used for the optical studies in back-reflection configuration (shown above in Figure4.3).

Figure4.5 (b) shows the photoluminescence image of DAAQ mesowire captured through the top channel. The bright photoluminescence spot is an excitation end and the emission end of mesowire is indicated by white dashed circle. The corresponding back focal image of emission was captured using the top channel which is shown in Figure4.5(c). The emission profile also characterized as a function of the azimuthal and radial distribution of the light intensity in the BFP image, shown in Figure4.5(d, e). The inset in (e) shows the white dashed line along which the light intensity was calculated. An important inference that we can draw from this observation is that the emission angles differ when compared to reflection mode (see Figure4.3). Such differences mainly

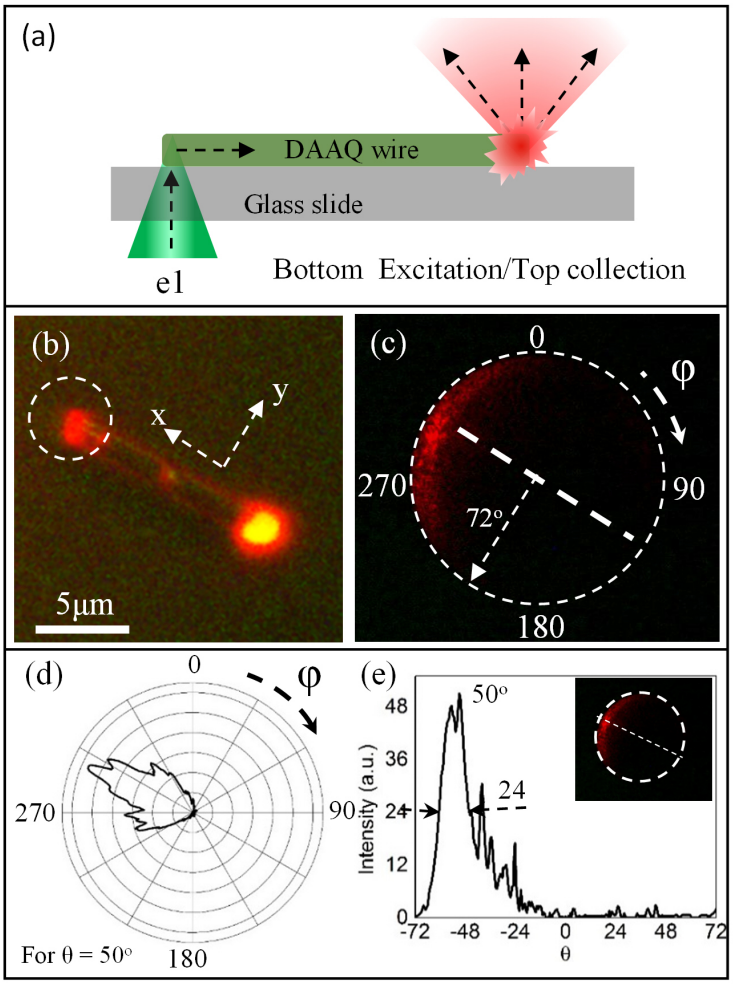

FIGURE 4.5: The waveguided Frenkel-exciton emission of DAAQ wire has been observed in the transmission configuration of dual channel microscopy system. The PL emission was collected from top channel where the DAAQ were illuminated through the bottom channel. (a) Shows the schematic of excitation and collection configuration. (b) shows the photoluminescence image of DAAQ wire which is illuminated using bottom-channel. The emission end is indicated with the white dashed circle whereas the big bright spot is an excitation end. (c) Corresponding back focal image (BFP) of spatial filtered photoluminescence emission from the distal end of DAAQ wire. The dashed line in image represents the orientation of DAAQ wire. The polar plot of emission intensity distribution along the azimuthal angle at a constant polar angle as shown in (d). The radial distribution of emission intensity was also quantified as shown in (e). The linear plot indicates that the maximum emission occurs between 40 ^{o} to 70 ^{o}.

arise due to the contrast in the refractive index at the interface and has to be taken to be account while quantifying angular emission. This emphasizes the relevance of performing and comparing Fourier plane imaging in reflection and transmission mode and

configuration has to be considered judiciously based on the design of optical device.

4.3.4 Fabry-Perot modes characterization using both channels

An interesting characteristic of organic mesowire waveguide is that it facilitates Fabry-Perot (F-P) resonances [170]. In the present context, we were interested to know if the F-P spectral features measured from the bottom and top channel vary. To probe this, we recorded higher resolution PL spectra from the bottom and top channel configuration (see stacked spectra in Figure4.6a).

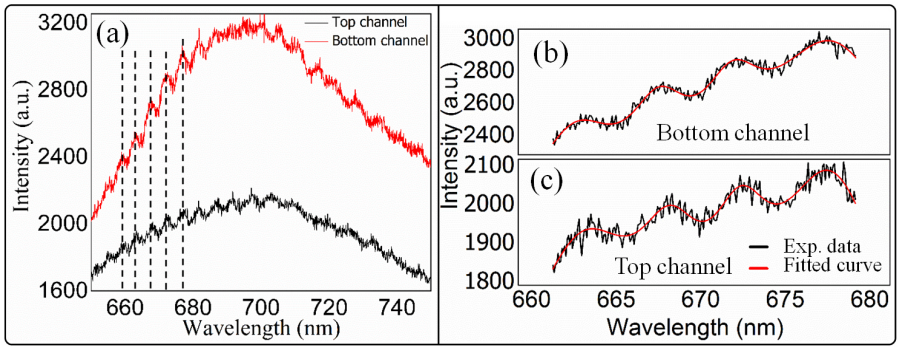

FIGURE 4.6: (a) Comparison of Fabry-Perot modes in the PL emission from bottom and top channels. The dotted lines are guides for the eye. Lorentzian fits for four of the FP modes analyzed for the emission captured from (b) bottom and (c) top optical channels.

We observed that the spectral intensity for bottom-channel due to two reasons: variation in numerical aperture of the objective lenses and pronounced radiative emission into medium of higher dielectric at an interface (bottom channel, in present case) configuration was higher than lower channel, which may be Next, we compared the F-P mode positions for the two recorded spectra and found that their peaks matched (see dotted lines in Figure4.6a). This confirms that the free-spectral range[193] of the F-P waveguide resonator does not vary on the medium of measurement. Interesting, the finesse of the cavity [193], which was measured by determining the full-width at half maxima of individual F-P modes (see Lorentzian-fitted curves in Figure4.6b and c) did show a variation. The value of finesse for bottom and top channel measurements were found to be 0.85 and 0.96, respectively. This indicates that the top channel device operation facilitates a higher finesse compared to bottom channel, and may have implications for designing optical sensors based on F-P resonances of organic waveguides.

Versatility of dual channel Fourier microscopy and spectroscopy system

4.3.5 Surface plasmon polariton (SPP) assisted light propagation and directional emission in silver nanowire

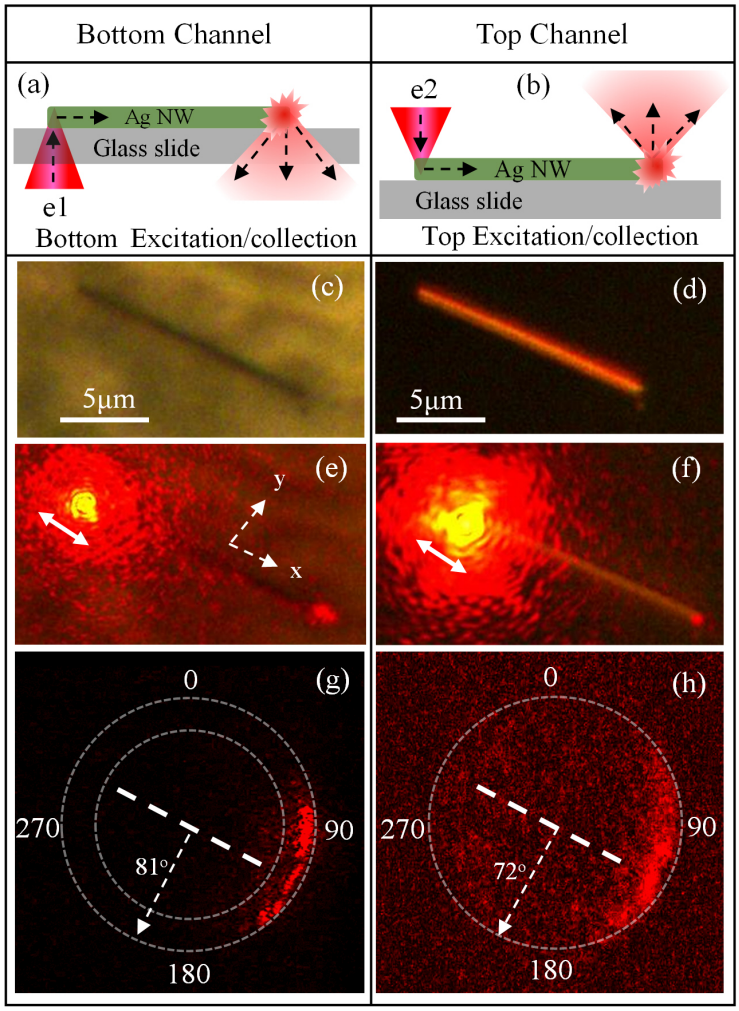

FIGURE 4.7: (a, b) Show the schematic of an experimental configuration of excitation and collection of signals. (c, d) bright-field optical image of a single silver nanowire captured through the bottom channel and top channel, respectively. (e, f) optical image of 632.8nm Laser excitation of Ag NW captured through both the channels. (g, h) shows the corresponding Fourier plane images of the emission from the distal end of Ag NW using the bottom channel and top channel, respectively. Here, the emission from the distal end was spatially filtered out using an aperture. Dashed line indicates the orientation of Ag NW.

In order to show the versatility of dual channel optical Fourier microscopy and spectroscopy instrument, we have analyzed the surface plasmon polariton (SPP) assisted light propagation and emission from the distal end of the silver nanowire (Ag NW). The Ag NW structures were prepared using seed-mediated protocol [194, 195]. The SPP excitation and collection of out-coupled photons from the distal of Ag NW were performed in back-scattered configuration, as shown in Figure4.7(a) and (b). The bright field optical image of silver nanowire captured through Figure4.7(c) bottom channel and Figure4.7(d) top channel, respectively.

By employing individual channel to excite plasmons at one end (big bright spot) of nanowire leads to the SPP propagation at the glass-metal interface and air-metal interface, respectively. Figure4.7 (e) and (f) show the single isolated silver nanowire system excited through the bottom channel and top channel, with the wavelength of 632.8nm laser light. The white arrow indicates the polarization of incident laser light. The spatial filtered back-reflection emission from the distal end was imaged in the Fourier plane of high numerical aperture objective lens of Figure4.7(g) bottom channel and Figure4.7(h) top channel. The BFP images of both channels clearly shows the difference in the emission pattern of light intensity into glass substrate and superstrate. There is a quantitative difference in the polar and azimuthal angles of scattered signals which is due to the contrast in the refractive index at the interface. Importantly, our dual channel microscope reveals the radial angular emission differes for the two measurement configurations and has to be taken into account while quantifying nanowire based directional emission. We note that such difference in directional emission as function of refractive index of medium on top a plasmonic nanowire has been studied previously [196]. In this study, we highlight that the difference in angular emission can be revealed even for the refractive index contrast observed at the interface.

4.3.6 Photoluminescence directional emission from the few-layer MoS_2 flake

We have observed the photoluminescence emission pattern from the isolated few-layer MoS_2 flake using back-scattered configuration, as shown in Figure4.8(a). The few layer flake were obtained by mechanical exfoliation using scotch tape technique on the optically transparent substrate (glass cover slip). The isolated flake was identified using bottom channel of the optical microscope. To observe the bright-field optical image, the top channel was used to illuminate white light which essentially create the optical contrast between flake and transparent substrate, as shown in Figure4.8(b). For the photoluminescence (PL) excitation, we used tightly focused 532nm laser light through the glass substrate using bottom channel. The back-scattered PL were collected through

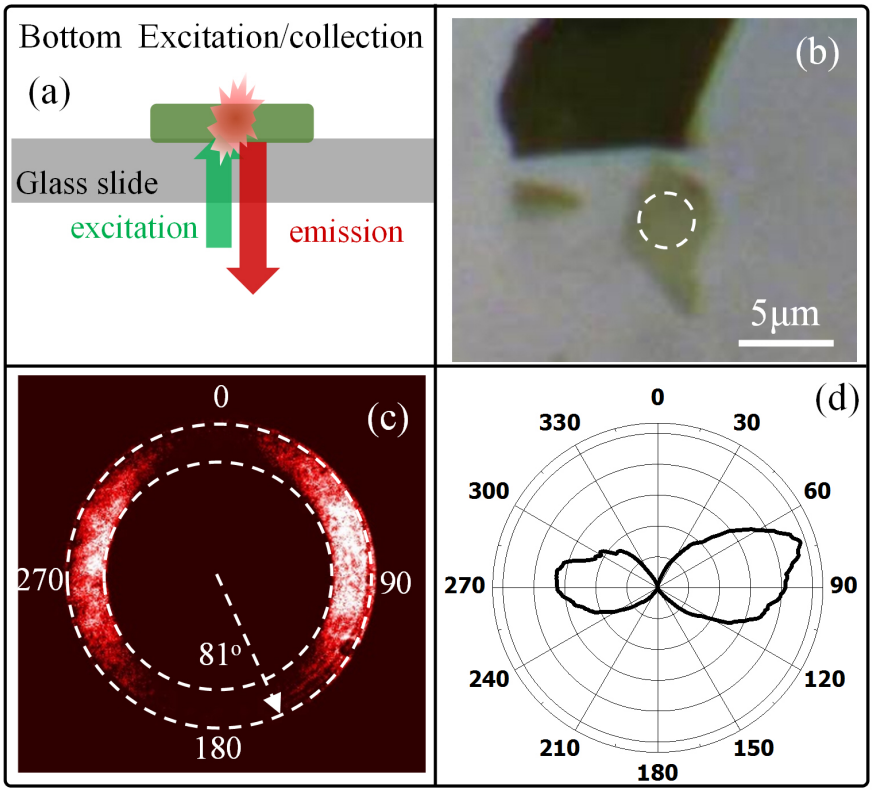

FIGURE 4.8: (a) Comparison of Fabry-Perot modes in the PL emission from bottom and top channels. The dotted lines are guides for the eye. Lorentzian fits for four of the FP modes analyzed for the emission captured from (b) bottom and (c) top optical channels.

the same channel and routed towards the CCD at conjugate BFP of the objective lens, represented in Figure4.8 (c).

In order to further quantify the emission property, we plotted the intensity distribution along the azimuthal angle at a constant polar angle (52^o) shown in (d). It can be observed that the emission from the central part of MoS_2 flake shows the symmetric lobes in the Fourier plane. Such emission pattern shows the in-plane dipolar emission from the excitons oriented in the MoS_2 flake [197]. An important aspect of our work is that the measurement was performed through a transparent glass substrate which is a medium of higher refractive index compared to the superstrate (air in this case). In the previous study [197] the PL emission from MoS_2 flake was performed in the reflection mode where the illumination and collection were performed using a lower NA lens. Whereas, in our case the emission directionality was quantified using a higher NA lens (1.49). An important advantage in our case is that the emission intensity is greater compared to the previous study as the PL was collected through the medium of higher refractive index. In addition to this, our configuration can be harnessed to probe angular

PL emission from 2D materials even in the presence of external perturbations such as electrical contacts and fluid motion.

4.4 Conclusion

To conclude, we have studied angular PL emission characteristics of the waveguided exciton-polaritons from distal ends of an organic mesowire placed at a dielectric interface, both through the reflection and transmission modes. We found the radial and azimuthal emission characteristics vary for experiments performed through the substrate and superstrate. Such variation in the emission angle has direct implication in engineering polariton emission characteristics of light emitting devices and has to be taken into account while designing light sources on a chip. Furthermore, our characterization of spectral features in the bottom and top channel configuration showed that the finesse of the Fabry-Perot spectral resonance varies depending upon the location of experimental measurement. Since finesse of cavity resonance is an important parameter in resonant sensors, our work clearly facilitates an optical microscopy/spectroscopy method to quantify these parameters with good accuracy. To show the versatility of our microscope, we quantified angular distribution of directional light scattering from a single plasmonic silver nanowire, and angular distribution of exciton photoluminescence from the MoS2 nanolayers through the transparent glass substrate. An interesting direction to explore would be the nonlinear optical emission from such individual organic waveguide resonators and see how the angular emission varies at a dielectric-dielectric interface and dielectric-plasmon interface.

Chapter 5

Summary and Future Directions

Controlling electromagnetic fields at nanoscale is an important property in the perspective of various applications. Light manipulations at sub-wavelength regime have been studied in plasmonic nanostructures. Coupling of light with the collective oscillations of free electrons at the surface of metal nanostructures enables confinement and propagation of electromagnetic fields beyond the diffraction limit. With this hindsight, we have explored the light propagation, localization and emission characteristics of coupled plasmonic nanostructure architectures. The work presented in this thesis is mainly focused on the manipulation of light propagation and directional emission from coupled nanowires systems using home-built Fourier optical microscopy and spectroscopy instrument.

In chapter 2, we have shown the light propagation and emission properties in the end-to-end conductively coupled silver nanowires. We have studied the new kind of geometry where two wires are conductively coupled with each other in the shape of English alphabet "V" with different angles. The incident light polarization and angle between nanowires of this geometry play the critical role in the light propagation and emission from the junction and distal end. Such nano-plasmonic configurations can be employed as plasmonic circuit elements for on-chip nanophotonics and plasmon resonance tunneling. The work includes the single excitation wavelength (632.81 nm) to create plasmons at the ends and junctions, respectively. Such structures can also be employed for multiple excitation wavelengths, the geometry can be extrapolated to realize multicolor light routing. This unique geometry of plasmonic nanostructure can be harnessed for multiple channels for light routing, where the junction and distal end of Ag NW can be further utilized as nanoscale light sources.

In the next chapter, we have studied the silver nanowire-nanoparticle (Ag NW-NP) system to probe the directional emission from the NW-NP junction using dual-excitation capability. This hybrid nanostructure system was formed by self-assembled process where a silver nanoparticle placed in the vicinity of the surface of silver nanowire.

Such systems show promising results of directional emissions which can address important and potential applications like optical nano-antennas. In this work, we have shown the single- and dual-channel optical antenna property of Ag NW-NP system that can influence directivity of elastic scattering and fluorescence emission of molecules. For the future direction, it would be interesting to observe the directional nature of single photon emission from a single emitter such as a single fluorophore, quantum dots and nitrogen-vacancy in diamond, close to the NW-NP junction. The mode volume NW-NP junction is very small, it would interesting to observe the Purcell enhancement factor. The coupled plasmonic nanostructure geometries not only enhance the rate of spontaneous emission from emitters but also influence their directionality of emission.
The last section of the thesis work presents the angular PL emission characteristics of the waveguided exciton-polaritons from the distal end of DAAQ mesowire system placed at the dielectric interface. We observed the variation in the radial and azimuthal emission characteristics for experiments performed through the substrate and superstrate. This kind of observation has implication in engineering polariton emission of light emitting device for designing light sources on a chip. We have also characterized the spectral features of emission using the bottom channel and top channel configuration. It was observed that the finesse of the Fabry-Perot spectral resonance varies for the PL emission through the dielectric substrate and from the superstrate. For the future direction, it would be interesting to explore the nonlinear optical emission from the organic waveguide resonator which can reveal the variation of angular emission profiles at the dielectric-dielectric interface and dielectric-plasmon interface. To address such issues, the experiments are underway in our laboratory.

Appendix A

Appendix A

For the detailed calculations of surface plasmons modes, we have solved the Maxwell equation. In the calculations, we have considered the cylinder of radius R with dielectric permittivity ϵ_2, which is aligned towards the z-axis and surrounded by a dielectric medium of dielectric permittivity ϵ_1 . The medium was considered non-magnetic and hence μ = 1 for each medium. For the calculation of surface modes, we have solved the wave equation given by

$$\nabla^2 E(r) + \frac{\omega^2}{c^2}\epsilon(r)E(r) = 0 \tag{A.1}$$

$$\nabla^2 H(r) + \frac{\omega^2}{c^2}\epsilon(r)H(r) = 0 \tag{A.2}$$

In order to solve the above equation, we have chosen the cylindrical coordinates. The solution of the equation 1 and 2 have calculated first the scalar solutions and then it was generalized in vector solutions. The following is the solution of above equation

$$\psi_1 \propto H_m(k_{1\perp}\rho)\exp^{im\phi+ik_{||}z} \tag{A.3}$$

$$\psi_2 \propto J_m(k_{2\perp}\rho)\exp^{im\phi+ik_{||}z} \tag{A.4}$$

ψ_1 and ψ_2 are scalar solutions, satisfying the necessary boundary conditions, outside and inside the cylinder, respectively. J_m and H_m are Bessel function and Hankel functions if the first kind, respectively. And,

$$k_{1\perp} = \sqrt{k_i^2 + k_{||}^2} \tag{A.5}$$

$$k_i = \omega\frac{\sqrt{\epsilon}}{c} \tag{A.6}$$

Here, for the large x, J_m well behaved at ρ=0 and $H_m(x) \quad e^{ix}$. Now, the vector solutions of the equations 1 and 2 are of the form:

$$V_i = \frac{1}{k_i}\nabla X(\hat{z}\psi) \tag{A.7}$$

$$W_i = \frac{1}{k_i}\nabla X\nu_i \tag{A.8}$$

For the solution of the above vector equations, we have got the following electric field and magnetic field expressions by solving curl relations of Maxwell equations is given by:

$$E_i(r) = a_i\nu_i(r) + b_iw_i(r) \tag{A.9}$$

$$H_i(r) = -\frac{i}{\omega\mu_o}k_i[a_iw_i(r) + b_i\nu_i(r)] \tag{A.10}$$

a_i and b_i are constant coefficients.

The detail expressions of E and H are given below:

$$E_i(r) = \Big\{[\frac{im}{k_i\rho}a_iF_{i,m}(k_{1\perp}\rho) + \frac{ik_{||}k_{i\perp}}{k_i^2}b_iF_{i,m}^{'}(k_{1\perp}\rho)]\hat{\rho} + [-\frac{k_{i\perp}}{k_i}a_iF_{i,m}^{'}(k_{1\perp}\rho) - \frac{mk_{||}k_i^2\rho}{b}{}_iF_{i,m}(k_{i\perp})]\hat{\phi}$$
$$+ \frac{k_{i\perp}^2}{k_i^2}b_iF_{i,m}^{'}(k_{1\perp}\rho)\hat{z}e^{im\phi+ik_{||}z} \tag{A.11}$$

$$H_i(r) = -\frac{i}{\omega\mu_o}k_i[\frac{im}{k_i\rho}b_iF_{i,m}(k_{1\perp}\rho) + \frac{ik_{||}k_{i\perp}}{k_i^2}a_iF_{i,m}^{'}(k_{1\perp}\rho)]\hat{\rho} + [-\frac{k_{i\perp}}{k_i}b_iF_{i,m}^{'}(k_{1\perp}\rho) - \frac{mk_{||}k_i^2\rho}{b}{}_iF_{i,m}(k_{i\perp})]\hat{\phi}$$
$$+ \frac{k_{i\perp}^2}{k_i^2}a_iF_{i,m}^{'}(k_{1\perp}\rho)\hat{z}e^{im\phi+ik_{||}z} \tag{A.12}$$

Here,

$F_{1,m}(x) = H_m(x)$ and $F_{2,m}(x) = J_m(x)$

a_i and b_i can be determined by using boundary conditions. Now, the tangential component E_ϕ, E_z , H_ϕ and H_z of the fields should be continuous at the metal-dielectric interface which will give the linear system of four equations which can be written in the abbreviated form:

$$M \left\{ \begin{array}{c} \mathrm{a}_1 \\ \mathrm{a}_2 \\ \mathrm{b}_1 \\ \mathrm{b}_2 \end{array} \right\} = 0$$

By setting up the det(M) = 0 gives the non-trivial solutions. The mode equation obtains after some simplifications of the above equation, given below:

$$\frac{m^2 k_{||}^2}{R^2}\left(\frac{1}{k_{M\perp}^2} - \frac{1}{k_{D\perp}^2}\right) = \left[\frac{1}{k_{D\perp}} \frac{J_m^{'}(k_{M\perp}R)}{J_m(k_{M\perp}R)} - \left[\frac{1}{k_{D\perp}} \frac{H_m^{'}(k_{D\perp}R)}{H_m(k_{D\perp}R)}\right] X \left[\frac{k_M^2}{k_{M\perp}} \frac{J_m^{'}(k_{M\perp}R)}{J_m(k_{M\perp}R)} - \frac{k_D^2}{k_{D\perp}} \frac{H_m^{'}(k_{D\perp}R)}{H_m(k_{D\perp}R)}\right] \tag{A.13}$$

The above equation gives the allowed values of $k_{||}$ as a function of m, R and ϵ_i.

A.0.1 Analysis of fundamental mode (m = 0)

For $m = 0$, one of the terms on the right side of the equation A.13 has to be zero. By setting first term to be zero corresponds to the transverse electric (TE) mode whereas, setting second terms to zero corresponds to the transverse magnetic (TM) mode. This property can be check by analyzing the equation A.11 and equation A.12, respectively. The TE mode equation does not have any solutions and hence fundamental mode at $m = 0$ is TM mode.

The simplified form of the equation is:

$$\frac{k_2^2}{k_{2\perp}} \frac{J_0^{'}(k_{2\perp}R)}{J_0(k_{2\perp}R)} - \frac{k_1^2}{k_{1\perp}} \frac{H_0^{'}(k_{1\perp}R)}{H_0(k_{1\perp}R)} = 0 \tag{A.14}$$

Here, $D = 1$ (represents the dielectric medium which is outside medium of cylinder) and $M = 2$ (represents the metallic medium). The electric and magnetic field distribution for this mode (no winding, $m = 0$) where H along z vanishes which implies the coefficient $a_i = 0$. By using this condition the expresions for $E(r)$ and $H(r)$ is given below:

$$E_D = b_D\left[\frac{ik_{||}k_{D\perp}}{k_D^2} H_0^{'}(k_{D\perp}\rho)\hat{\rho} + \frac{k_{D\perp}^2}{k_D^2} H_0(k_{D\perp}\rho)\hat{z}\right] e^{ik_{||}z} \tag{A.15}$$

$$E_M = b_M\left[\frac{Jk_{||}k_{D\perp}}{k_M^2} J_0^{'}(k_{M\perp}\rho)\hat{\rho} + \frac{k_{M\perp}^2}{k_M^2} J_0(k_{M\perp}\rho)\hat{z}\right] e^{ik_{||}z} \tag{A.16}$$

$$H_D = \frac{j}{\omega\mu_o} k_{D\perp} b_D H_0^{'}(k_{D\perp}\rho) e^{jk_{||}z}\hat{\phi} \tag{A.17}$$

$$H_M = \frac{j}{\omega\mu_o} k_{M\perp} b_M H_0^{'}(k_{M\perp}\rho) e^{jk_{||}z}\hat{\phi} \tag{A.18}$$

There is no cut-off value for m=0 mode it is quasi-static configuration of field and it is axially symmetric transverse magnetic mode [198].

A.0.2 Analysis of mode (m = 1)

In the case of $m = 1$, it is very important to study it quite carefully because this mode does not have any strictly cut off value of radius of nanowire. In this mode as $R \to 0$ $k_{||} \to \sqrt{\epsilon_1}$ exponentially. The magnitude of $k_{1\perp}$becomes exponentially small which indicates the mode volume and spatial extent of growth of field. In order to solve the mode equation, it is important to define new factor to approximate the solutions in the limit of small value.

$$\delta = k_\perp - \sqrt{\epsilon_1} \tag{A.19}$$

The both sides of equation A.13 (mode equation) were expanded separately. The left side has the following form:

$$LHS = \frac{1}{4R^2\delta^2} - \frac{(3\epsilon_1 + \epsilon_2)}{4R^2\sqrt{\epsilon_1}(\epsilon_1 - \epsilon_2)\delta} + O(\delta^0) \tag{A.20}$$

For the calculation of RHS, it is assumed that the quantities $k_{1\perp}R$ and $k_{1\perp}$ will be small as $R \to 0$. After solving by taking simplifications, RHS have the following form:

$$RHS = \frac{1}{4R^2\delta^2} - \frac{\epsilon_1 + 3\epsilon_2 - 2R^2\epsilon_1(\epsilon_1 - \epsilon_2)\log(\frac{\delta R^2\sqrt{\epsilon_1}}{2})}{4R^2\sqrt{\epsilon_1}(\epsilon_1 - \epsilon_2)\delta} \tag{A.21}$$

Now by equating the left and right-hand side expressions of $O\delta^(- 1)$ gives the following solution:

$$\delta = \frac{2}{R^2\delta^2}\exp[-\frac{2(\epsilon_1 + \epsilon_2)}{R^2\epsilon_1(\epsilon_1 - \epsilon_2)}] \tag{A.22}$$

It follows the nanowire limit,

$$\begin{aligned} k &= \sqrt{k_{||}^2 - \epsilon_D} \\ &\approx (2\delta\sqrt{\epsilon_D}) \\ &\approx \frac{2}{R}\exp[-\frac{2(\epsilon_1+\epsilon_2)}{R^2\epsilon_1(\epsilon_1-\epsilon_2)}] \end{aligned} \tag{A.23}$$

The above equation shows that the$m = 1$ mode does not have cut-off value in the nanowire limit but the longitudinal wave vector tend to $\sqrt{\epsilon_D}$ exponentially. Hence these mode are highly localized and does not propagate. The charge oscillations happens in the plane of horizontal and vertically perpendicular to the axis of nanowire [199, 200].

Bibliography

[1]M. C. Doherty, "Discovering the 'true form:'hooke's micrographia and the visual vocabulary of engraved portraits", Notes and Records of the Royal Society **66**, 211–234 (2012).

[2]R. Brown, "Xxvii. a brief account of microscopical observations made in the months of june, july and august 1827, on the particles contained in the pollen of plants; and on the general existence of active molecules in organic and inorganic bodies", Philosophical Magazine Series 2 **4**, 161–173 (1828).

[3]P. Török and F.-J. Kao, "Total internal reflection fluorescence microscopy", Optical Imaging and Microscopy: Techniques and Advanced Systems, 195–236 (2007).

[4]R. Wayne, "Light and video microscopy", (2009).

[5]C. Cremer and T. Cremer, "Considerations on a laser-scanning-microscope with high resolution and depth of field", Microscopica acta, 31–44 (1974).

[6]C. Cremer and T. Cremer, "Considerations on a laser-scanning-microscope with high resolution and depth of field", Microscopica acta, 31–44 (1974).

[7]D. W. Pohl, W Denk, and M Lanz, "Optical stethoscopy: image recording with resolution $\lambda/20$", Applied physics letters **44**, 651–653 (1984).

[8]M. G. Gustafsson, "Surpassing the lateral resolution limit by a factor of two using structured illumination microscopy", Journal of microscopy **198**, 82–87 (2000).

[9]C Hettich, C Schmitt, J Zitzmann, S Kühn, I Gerhardt, and V Sandoghdar, "Nanometer resolution and coherent optical dipole coupling of two individual molecules", Science **298**, 385–389 (2002).

[10]X. Qu, D. Wu, L. Mets, and N. F. Scherer, "Nanometer-localized multiple single-molecule fluorescence microscopy", Proceedings of the National Academy of Sciences of the United States of America **101**, 11298–11303 (2004).

[11]M. P. Gordon, T. Ha, and P. R. Selvin, "Single-molecule high-resolution imaging with photobleaching", Proceedings of the National Academy of Sciences of the United States of America **101**, 6462–6465 (2004).

[12]G. Donnert, J. Keller, R. Medda, M. A. Andrei, S. O. Rizzoli, R. Lührmann, R. Jahn, C. Eggeling, and S. W. Hell, "Macromolecular-scale resolution in biological fluorescence microscopy", Proceedings of the National Academy of Sciences **103**, 11440–11445 (2006).

[13]S. Bretschneider, C. Eggeling, and S. W. Hell, "Breaking the diffraction barrier in fluorescence microscopy by optical shelving", Physical review letters **98**, 218103 (2007).

[14]A. Pertsinidis, Y. Zhang, and S. Chu, "Subnanometre single-molecule localization, registration and distance measurements", Nature **466**, 647–651 (2010).

[15]J. C. Vaughan, S. Jia, and X. Zhuang, "Ultrabright photoactivatable fluorophores created by reductive caging", Nature methods **9**, 1181–1184 (2012).

[16]D. Wildanger, B. R. Patton, H. Schill, L. Marseglia, J. Hadden, S. Knauer, A. Schönle, J. G. Rarity, J. L. O'Brien, S. W. Hell, et al., "Solid immersion facilitates fluorescence microscopy with nanometer resolution and sub-ångström emitter localization", Advanced Materials **24** (2012).

[17]S. Weisenburger, B. Jing, D. Hänni, L. Reymond, B. Schuler, A. Renn, and V. Sandoghdar, "Cryogenic colocalization microscopy for nanometer-distance measurements", ChemPhysChem **15**, 763–770 (2014).

[18]G. V. Hartland, "Ultrafast studies of single semiconductor and metal nanostructures through transient absorption microscopy", Chemical Science **1**, 303–309 (2010).

[19]A. Furube, Y. Tamaki, and R. Katoh, "Transient absorption measurement of organic crystals with femtosecond-laser scanning microscopes", Journal of Photochemistry and Photobiology A: Chemistry **183**, 253–260 (2006).

[20]I. H. van Stokkum, D. S. Larsen, and R. van Grondelle, "Global and target analysis of time-resolved spectra", Biochimica et Biophysica Acta (BBA)-Bioenergetics **1657**, 82–104 (2004).

[21]A Maciejewski, R Naskrecki, M Lorenc, M Ziolek, J Karolczak, J Kubicki, M Matysiak, and M Szymanski, "Transient absorption experimental set-up with femtosecond time resolution. femto-and picosecond study of dcm molecule in cyclohexane and methanol solution", Journal of Molecular Structure **555**, 1–13 (2000).

[22]T. Virgili, G. Grancini, E. Molotokaite, I. Suarez-Lopez, S. K. Rajendran, A. Liscio, V. Palermo, G. Lanzani, D. Polli, and G. Cerullo, "Confocal ultrafast pump–probe spectroscopy: a new technique to explore nanoscale composites", Nanoscale **4**, 2219–2226 (2012).

[23]A. Crut, P. Maioli, N. Del Fatti, and F. Vallée, "Acoustic vibrations of metal nano-objects: time-domain investigations", Physics Reports **549**, 1–43 (2015).

[24]T. A. Major, S. S. Lo, K. Yu, and G. V. Hartland, "Time-resolved studies of the acoustic vibrational modes of metal and semiconductor nano-objects", The journal of physical chemistry letters **5**, 866–874 (2014).

[25]A. Crut, P. Maioli, N. Del Fatti, and F. Vallée, "Optical absorption and scattering spectroscopies of single nano-objects", Chemical Society Reviews **43**, 3921–3956 (2014).

[26]S. A. Maier, *Plasmonics: fundamentals and applications* (Springer Science & Business Media, 2007).

[27]A. A. Maradudin, J. R. Sambles, and W. L. Barnes, *Modern plasmonics*, Vol. 4 (Elsevier, 2014).

[28]C. Sheppard, "Super-resolution in confocal imaging", Optik **80**, 53–54 (1988).

[29]C. SHEPPARD and A CHOUDHURY, "Image formation in the scanning microscope", OPTICA ACTA **24**, 1051–1073 (1977).

[30]C. B. Müller and J. Enderlein, "Image scanning microscopy", Physical review letters **104**, 198101 (2010).

[31]S. W. Hell and J. Wichmann, "Breaking the diffraction resolution limit by stimulated emission: stimulated-emission-depletion fluorescence microscopy", Optics letters **19**, 780–782 (1994).

[32]T. A. Klar and S. W. Hell, "Subdiffraction resolution in far-field fluorescence microscopy", Optics letters **24**, 954–956 (1999).

[33]S. W. Hell, "Far-field optical nanoscopy", science **316**, 1153–1158 (2007).

[34]R. Heintzmann, T. M. Jovin, and C. Cremer, "Saturated patterned excitation microscopy—a concept for optical resolution improvement", JOSA A **19**, 1599–1609 (2002).

[35]S. Hell and E. H. Stelzer, "Properties of a 4pi confocal fluorescence microscope", JOSA A **9**, 2159–2166 (1992).

[36]S. Hell, M Schrader, and H. Van Der Voort, "Far-field fluorescence microscopy with three-dimensional resolution in the 100-nm range", Journal of microscopy **187**, 1–7 (1997).

[37]S. Hell and E. H. Stelzer, "Fundamental improvement of resolution with a 4pi-confocal fluorescence microscope using two-photon excitation", Optics Communications **93**, 277–282 (1992).

[38]M. Nagorni and S. W. Hell, "Coherent use of opposing lenses for axial resolution increase. ii. power and limitation of nonlinear image restoration", JOSA A **18**, 49–54 (2001).

[39]A. Egner and S. W. Hell, "Fluorescence microscopy with super-resolved optical sections", Trends in cell biology **15**, 207–215 (2005).

[40]B. L. Haas, J. S. Matson, V. J. DiRita, and J. S. Biteen, "Imaging live cells at the nanometer-scale with single-molecule microscopy: obstacles and achievements in experiment optimization for microbiology", Molecules **19**, 12116–12149 (2014).

[41]W. Min, S. Lu, S. Chong, R. Roy, G. R. Holtom, and X. S. Xie, "Imaging chromophores with undetectable fluorescence by stimulated emission microscopy", Nature **461**, 1105–1109 (2009).

[42]R. Berera, R. van Grondelle, and J. T. Kennis, "Ultrafast transient absorption spectroscopy: principles and application to photosynthetic systems", Photosynthesis research **101**, 105–118 (2009).

[43]U Megerle, I Pugliesi, C Schriever, C. Sailer, and E Riedle, "Sub-50 fs broadband absorption spectroscopy with tunable excitation: putting the analysis of ultrafast molecular dynamics on solid ground", Applied Physics B: Lasers and Optics **96**, 215–231 (2009).

[44]D. Davydova, A. Cadena, D. Akimov, and B. Dietzek, "Transient absorption microscopy: advances in chemical imaging of photoinduced dynamics", Laser & Photonics Reviews **10**, 62–81 (2016).

[45]V. I. Klimov, "Optical nonlinearities and ultrafast carrier dynamics in semiconductor nanocrystals", Journal of Physical Chemistry B **104**, 6112–6123 (2000).

[46]C Voisin, N. Fatti, D Christofilos, and F Vallee, "Ultrafast electron dynamics and optical nonlinearities in metal nanoparticles", J. Phys. Chem. B **105**, 2264–2280 (2001).

[47]J. Hodak, A Henglein, G. Hartland, et al., "Photophysics of nanometer sized metal particles: electron-phonon coupling and coherent excitation of breathing vibrational modes", Journal of Physical Chemistry B **104**, 9954–9965 (2000).

[48]M. A. van Dijk, M. Lippitz, and M. Orrit, "Detection of acoustic oscillations of single gold nanospheres by time-resolved interferometry", Physical review letters **95**, 267406 (2005).

[49]O. L. Muskens, N. Del Fatti, and F. Vallée, "Femtosecond response of a single metal nanoparticle", Nano letters **6**, 552–556 (2006).

[50]S. Berciaud, L. Cognet, G. A. Blab, and B. Lounis, "Photothermal heterodyne imaging of individual nonfluorescent nanoclusters and nanocrystals", Physical Review Letters **93**, 257402 (2004).

[51]S. Berciaud, L. Cognet, and B. Lounis, "Photothermal absorption spectroscopy of individual semiconductor nanocrystals", Nano letters **5**, 2160–2163 (2005).

[52]S. Berciaud, D. Lasne, G. A. Blab, L. Cognet, and B. Lounis, "Photothermal heterodyne imaging of individual metallic nanoparticles: theory versus experiment", Physical Review B **73**, 045424 (2006).

[53]M. Van Dijk, A. Tchebotareva, M. Orrit, M. Lippitz, S. Berciaud, D. Lasne, L. Cognet, and B. Lounis, "Absorption and scattering microscopy of single metal nanoparticles", Physical Chemistry Chemical Physics **8**, 3486–3495 (2006).

[54]D. Boyer, P. Tamarat, A. Maali, B. Lounis, and M. Orrit, "Photothermal imaging of nanometer-sized metal particles among scatterers", Science **297**, 1160–1163 (2002).

[55]M. Selmke, M. Braun, and F. Cichos, "Photothermal single-particle microscopy: detection of a nanolens", ACS nano **6**, 2741–2749 (2012).

[56]S. Berciaud, L. Cognet, and B. Lounis, "Luminescence decay and the absorption cross section of individual single-walled carbon nanotubes", Physical Review Letters **101**, 077402 (2008).

[57]A Gaiduk, M Yorulmaz, P. Ruijgrok, and M Orrit, "Room-temperature detection of a single molecule's absorption by photothermal contrast", Science **330**, 353–356 (2010).

[58]E. Ozbay, "Plasmonics: merging photonics and electronics at nanoscale dimensions", science **311**, 189–193 (2006).

[59]H. A. Atwater and A. Polman, "Plasmonics for improved photovoltaic devices", Nature materials **9**, 205–213 (2010).

[60]M. E. Stewart, C. R. Anderton, L. B. Thompson, J. Maria, S. K. Gray, J. A. Rogers, and R. G. Nuzzo, "Nanostructured plasmonic sensors", Chemical reviews **108**, 494–521 (2008).

[61]J. Wang, "A review of recent progress in plasmon-assisted nanophotonic devices", Frontiers of Optoelectronics **7**, 320–337 (2014).

[62]Z. Fang and X. Zhu, "Plasmonics in nanostructures", Advanced Materials **25**, 3840–3856 (2013).

[63]R. Chang, *Surface enhanced raman scattering* (Springer Science & Business Media, 2013).

[64]P. L. Stiles, J. A. Dieringer, N. C. Shah, and R. P. Van Duyne, "Surface-enhanced raman spectroscopy", Annu. Rev. Anal. Chem. **1**, 601–626 (2008).

[65]E. Fort and S. Grésillon, "Surface enhanced fluorescence", Journal of Physics D: Applied Physics **41**, 013001 (2007).

[66]J. R. Lakowicz, C. D. Geddes, I. Gryczynski, J. B. Malicka, Z. Gryczynski, K. Aslan, J. Lukomska, and J. Huang, "Advances in surface-enhanced fluorescence", in Biomedical optics 2004 (International Society for Optics and Photonics, 2004), pp. 10–28.

[67]M. Moskovits, "Surface-enhanced spectroscopy", Reviews of modern physics **57**, 783 (1985).

[68]D. Stuart, A. Haes, C. Yonzon, E. Hicks, and R. Van Duyne, "Biological applications of localised surface plasmonic phenomenae", in Iee proceedings-nanobiotechnology, Vol. 152, 1 (IET, 2005), pp. 13–32.

[69]G. J. Nusz, S. M. Marinakos, A. C. Curry, A. Dahlin, F. Höök, A. Wax, and A. Chilkoti, "Label-free plasmonic detection of biomolecular binding by a single gold nanorod", Analytical chemistry **80**, 984–989 (2008).

[70]A. G. Brolo, "Plasmonics for future biosensors", Nature Photonics **6**, 709–713 (2012).

[71]X. Zhang and Z. Liu, "Superlenses to overcome the diffraction limit", Nature materials **7**, 435–441 (2008).

[72]S. Kawata, Y. Inouye, and P. Verma, "Plasmonics for near-field nano-imaging and superlensing", Nature Photonics **3**, 388–394 (2009).

[73]R.-M. Ma, R. F. Oulton, V. J. Sorger, G. Bartal, and X. Zhang, "Room-temperature sub-diffraction-limited plasmon laser by total internal reflection", Nature materials **10**, 110–113 (2011).

[74]M. T. Hill, M. Marell, E. S. Leong, B. Smalbrugge, Y. Zhu, M. Sun, P. J. Van Veldhoven, E. J. Geluk, F. Karouta, Y.-S. Oei, et al., "Lasing in metal-insulator-metal sub-wavelength plasmonic waveguides", Optics express **17**, 11107–11112 (2009).

[75]E. Cubukcu, E. A. Kort, K. B. Crozier, and F. Capasso, "Plasmonic laser antenna", Applied Physics Letters **89**, 093120 (2006).

[76]P. Bharadwaj, B. Deutsch, and L. Novotny, "Optical antennas", Advances in Optics and Photonics **1**, 438–483 (2009).

[77]L. Novotny and N. Van Hulst, "Antennas for light", Nature photonics **5**, 83–90 (2011).

[78]R. Ritchie, "Plasma losses by fast electrons in thin films", Physical Review **106**, 874 (1957).

[79]D. Pines and D. Bohm, "A collective description of electron interactions: ii. collective vs individual particle aspects of the interactions", Physical Review **85**, 338 (1952).

[80]D. Pines, "Collective energy losses in solids", Reviews of modern physics **28**, 184 (1956).

[81]C. Powell and J. Swan, "Origin of the characteristic electron energy losses in aluminum", Physical Review **115**, 869 (1959).

[82]C. Powell and J. Swan, "Origin of the characteristic electron energy losses in magnesium", Physical Review **116**, 81 (1959).

[83]E. Stern and R. Ferrell, "Surface plasma oscillations of a degenerate electron gas", Physical Review **120**, 130 (1960).

[84]C. F. Bohren and D. R. Huffman, *Absorption and scattering of light by small particles* (John Wiley & Sons, 2008).

[85]C.-H. Chou and F.-C. Chen, "Plasmonic nanostructures for light trapping in organic photovoltaic devices", Nanoscale **6**, 8444–8458 (2014).

[86]K. L. KELLY, E. CORONADO, L. L. ZHAO, and G. C. SCHATZ, "The optical properties of metal nanoparticles: the influence of size, shape, and dielectric environment", The Journal of physical chemistry. B **107**, 668–677 (2003).

[87]M. D. Malinsky, K. L. Kelly, G. C. Schatz, and R. P. Van Duyne, "Chain length dependence and sensing capabilities of the localized surface plasmon resonance of silver nanoparticles chemically modified with alkanethiol self-assembled monolayers", Journal of the American Chemical Society **123**, 1471–1482 (2001).

[88]W. L. Barnes, A. Dereux, and T. W. Ebbesen, "Surface plasmon subwavelength optics", Nature **424**, 824–830 (2003).

[89]L. J. Sherry, S.-H. Chang, G. C. Schatz, R. P. Van Duyne, B. J. Wiley, and Y. Xia, "Localized surface plasmon resonance spectroscopy of single silver nanocubes", Nano letters **5**, 2034–2038 (2005).

[90]A. V. Zayats, I. I. Smolyaninov, and A. A. Maradudin, "Nano-optics of surface plasmon polaritons", Physics reports **408**, 131–314 (2005).

[91]S. Kawata, *Near-field optics and surface plasmon polaritons*, Vol. 81 (Springer Science & Business Media, 2001).

[92]H. Raether, *Surface plasmons on smooth surfaces* (Springer, 1988).

[93]O. Benson, "Assembly of hybrid photonic architectures from nanophotonic constituents", Nature **480**, 193–199 (2011).

[94]D. E. Chang, A. S. Sørensen, P. Hemmer, and M. Lukin, "Strong coupling of single emitters to surface plasmons", Physical Review B **76**, 035420 (2007).

[95]J. A. Stratton, *Electromagnetic theory* (John Wiley & Sons, 2007).

[96]J. D. Jackson, *Electrodynamics* (Wiley Online Library, 1975).

[97]J. A. McKay and J. A. Rayne, "Temperature dependence of the infrared absorptivity of the noble metals", Physical Review B **13**, 673 (1976).

[98]A. Otto, "Excitation of nonradiative surface plasma waves in silver by the method of frustrated total reflection", Zeitschrift für Physik **216**, 398–410 (1968).

[99]E. Kretschmann, "Die bestimmung optischer konstanten von metallen durch anregung von oberflächenplasmaschwingungen", Zeitschrift für Physik A Hadrons and Nuclei **241**, 313–324 (1971).

[100]H. Raether, *Surface plasmons on smooth surfaces* (Springer, 1988).

[101]A. G. Curto, G. Volpe, T. H. Taminiau, M. P. Kreuzer, R. Quidant, and N. F. van Hulst, "Unidirectional emission of a quantum dot coupled to a nanoantenna", Science **329**, 930–933 (2010).

[102]J. R. Lakowicz, "Radiative decay engineering 3. surface plasmon-coupled directional emission", Analytical biochemistry **324**, 153–169 (2004).

[103]I. Gryczynski, J. Malicka, Z. Gryczynski, and J. R. Lakowicz, "Radiative decay engineering 4. experimental studies of surface plasmon-coupled directional emission", Analytical biochemistry **324**, 170–182 (2004).

[104]T. Shegai, V. D. Miljkovic, K. Bao, H. Xu, P. Nordlander, P. Johansson, and M. Kall, "Unidirectional broadband light emission from supported plasmonic nanowires", Nano letters **11**, 706–711 (2011).

[105]L. Novotny and B. Hecht, *Principles of nano-optics* (Cambridge university press, 2012).

[106]P. Nanoguides, "Circuits, edited by si bozhevolnyi", Pan Stanford, Singapore (2009).

[107]M. L. Brongersma and P. G. Kik, *Surface plasmon nanophotonics* (Springer, 2007).

[108]W. L. Barnes, A. Dereux, and T. W. Ebbesen, "Surface plasmon subwavelength optics", Nature **424**, 824–830 (2003).

[109]S. A. Maier, *Plasmonics: fundamentals and applications* (Springer Science & Business Media, 2007).

[110]T. W. Ebbesen, C. Genet, and S. I. Bozhevolnyi, "Surface-plasmon circuitry", Physics Today (2008).

[111]S. Lal, S. Link, and N. J. Halas, "Nano-optics from sensing to waveguiding", Nature photonics **1**, 641–648 (2007).

[112]H. Ditlbacher, A. Hohenau, D. Wagner, U. Kreibig, M. Rogers, F. Hofer, F. R. Aussenegg, and J. R. Krenn, "Silver nanowires as surface plasmon resonators", Physical review letters **95**, 257403 (2005).

[113]A. W. Sanders, D. A. Routenberg, B. J. Wiley, Y. Xia, E. R. Dufresne, and M. A. Reed, "Observation of plasmon propagation, redirection, and fan-out in silver nanowires", Nano letters **6**, 1822–1826 (2006).

[114]A. Akimov, A Mukherjee, C. Yu, D. Chang, A. Zibrov, P. Hemmer, H Park, and M. Lukin, "Generation of single optical plasmons in metallic nanowires coupled to quantum dots", Nature **450**, 402–406 (2007).

[115]A. L. Pyayt, B. Wiley, Y. Xia, A. Chen, and L. Dalton, "Integration of photonic and silver nanowire plasmonic waveguides", Nature nanotechnology **3**, 660–665 (2008).

[116]R. Yan, P. Pausauskie, J. Huang, and P. Yang, "Direct photonic–plasmonic coupling and routing in single nanowires", Proceedings of the National Academy of Sciences **106**, 21045–21050 (2009).

[117]Y. Fang, Z. Li, Y. Huang, S. Zhang, P. Nordlander, N. J. Halas, and H. Xu, "Branched silver nanowires as controllable plasmon routers", Nano letters **10**, 1950–1954 (2010).

[118]W. Wang, Q. Yang, F. Fan, H. Xu, and Z. L. Wang, "Light propagation in curved silver nanowire plasmonic waveguides", Nano letters **11**, 1603–1608 (2011).

[119]R. Chikkaraddy, D. Singh, and G. Pavan Kumar, "Plasmon assisted light propagation and raman scattering hot-spot in end-to-end coupled silver nanowire pairs", Applied Physics Letters **100**, 043108 (2012).

[120]C.-L. Zou, F.-W. Sun, Y.-F. Xiao, C.-H. Dong, X.-D. Chen, J.-M. Cui, Q Gong, Z.-F. Han, and G.-C. Guo, "Plasmon modes of silver nanowire on a silica substrate", Applied Physics Letters **97**, 183102 (2010).

[121]H. Wei, Z. Wang, X. Tian, M. Käll, and H. Xu, "Cascaded logic gates in nanophotonic plasmon networks", Nature Communications **2**, 387 (2011).

[122]S. J. Lee, J. M. Baik, and M. Moskovits, "Polarization-dependent surface-enhanced raman scattering from a silver-nanoparticle-decorated single silver nanowire", Nano letters **8**, 3244–3247 (2008).

[123]J. M. Baik, S. J. Lee, and M. Moskovits, "Polarized surface-enhanced raman spectroscopy from molecules adsorbed in nano-gaps produced by electromigration in silver nanowires", Nano letters **9**, 672–676 (2009).

[124]Y. Fang, H. Wei, F. Hao, P. Nordlander, and H. Xu, "Remote-excitation surface-enhanced raman scattering using propagating ag nanowire plasmons", Nano letters **9**, 2049–2053 (2009).

[125]T. Shegai, Y. Huang, H. Xu, and M. Käll, "Coloring fluorescence emission with silver nanowires", Applied Physics Letters **96**, 103114 (2010).

[126]S. Zhang, H. Wei, K. Bao, U. Håkanson, N. J. Halas, P. Nordlander, and H. Xu, "Chiral surface plasmon polaritons on metallic nanowires", Physical review letters **107**, 096801 (2011).

[127]Y. Sun, Y. Yin, B. T. Mayers, T. Herricks, and Y. Xia, "Uniform silver nanowires synthesis by reducing agno3 with ethylene glycol in the presence of seeds and poly (vinyl pyrrolidone)", Chemistry of Materials **14**, 4736–4745 (2002).

[128]D. E. Chang, A. S. Sørensen, P. Hemmer, and M. Lukin, "Strong coupling of single emitters to surface plasmons", Physical Review B **76**, 035420 (2007).

[129]S. Sidorenko and O. J. Martin, "Resonant tunneling of surface plasmon-polaritons", Optics express **15**, 6380–6388 (2007).

[130]S. A. Maier, *Plasmonics: fundamentals and applications* (Springer Science & Business Media, 2007).

[131]D. E. Chang, A. S. Sørensen, P. Hemmer, and M. Lukin, "Strong coupling of single emitters to surface plasmons", Physical Review B **76**, 035420 (2007).

[132]X. Xiong, C.-L. Zou, X.-F. Ren, A.-P. Liu, Y.-X. Ye, F.-W. Sun, and G.-C. Guo, "Silver nanowires for photonics applications", Laser & Photonics Reviews **7**, 901–919 (2013).

[133]X. Guo, Y. Ma, Y. Wang, and L. Tong, "Nanowire plasmonic waveguides, circuits and devices", Laser & Photonics Reviews **7**, 855–881 (2013).

[134]S. Lal, J. H. Hafner, N. J. Halas, S. Link, and P. Nordlander, "Noble metal nanowires: from plasmon waveguides to passive and active devices", Accounts of chemical research **45**, 1887–1895 (2012).

[135]H. Wei and H. Xu, "Nanowire-based plasmonic waveguides and devices for integrated nanophotonic circuits", Nanophotonics **1**, 155–169 (2012).

[136]B. Wild, L. Cao, Y. Sun, B. P. Khanal, E. R. Zubarev, S. K. Gray, N. F. Scherer, and M. Pelton, "Propagation lengths and group velocities of plasmons in chemically synthesized gold and silver nanowires", ACS nano **6**, 472–482 (2012).

[137]H. Ditlbacher, A. Hohenau, D. Wagner, U. Kreibig, M. Rogers, F. Hofer, F. R. Aussenegg, and J. R. Krenn, "Silver nanowires as surface plasmon resonators", Physical review letters **95**, 257403 (2005).

[138]H. Wei, Z. Wang, X. Tian, M. Käll, and H. Xu, "Cascaded logic gates in nanophotonic plasmon networks", Nature Communications **2**, 387 (2011).

[139]K. J. Russell, T.-L. Liu, S. Cui, and E. L. Hu, "Large spontaneous emission enhancement in plasmonic nanocavities", Nature Photonics **6**, 459–462 (2012).

[140]A. Akimov, A Mukherjee, C. Yu, D. Chang, A. Zibrov, P. Hemmer, H Park, and M. Lukin, "Generation of single optical plasmons in metallic nanowires coupled to quantum dots", Nature **450**, 402–406 (2007).

[141]S. Kumar, A. Huck, Y.-W. Lu, and U. L. Andersen, "Coupling of single quantum emitters to plasmons propagating on mechanically etched wires", Optics letters **38**, 3838–3841 (2013).

[142]A. Huck, S. Kumar, A. Shakoor, and U. L. Andersen, "Controlled coupling of a single nitrogen-vacancy center to a silver nanowire", Physical review letters **106**, 096801 (2011).

[143]M. W. Knight, N. K. Grady, R. Bardhan, F. Hao, P. Nordlander, and N. J. Halas, "Nanoparticle-mediated coupling of light into a nanowire", Nano Letters **7**, 2346–2350 (2007).

[144]N. P. De Leon, M. D. Lukin, and H. Park, "Quantum plasmonic circuits", IEEE Journal of Selected Topics in Quantum Electronics **18**, 1781–1791 (2012).

[145]D. Chang, A. S. Sørensen, P. Hemmer, and M. Lukin, "Quantum optics with surface plasmons", Physical review letters **97**, 053002 (2006).

[146]M. Song, A. Bouhelier, P. Bramant, J. Sharma, E. Dujardin, D. Zhang, and G. Colas-des Francs, "Imaging symmetry-selected corner plasmon modes in penta-twinned crystalline ag nanowires", ACS nano **5**, 5874–5880 (2011).

[147]Y. Sun, B. Gates, B. Mayers, and Y. Xia, "Crystalline silver nanowires by soft solution processing", Nano letters **2**, 165–168 (2002).

[148]A. Dasgupta, D. Singh, S. Tandon, R. P. Tripathi, and G. P. Kumar, "Remote-excitation surface-enhanced raman scattering with counter-propagating plasmons: silver nanowire-nanoparticle system", Journal of Nanophotonics **8**, 083899–083899 (2014).

[149]T. Shegai, V. D. Miljkovic, K. Bao, H. Xu, P. Nordlander, P. Johansson, and M. Kall, "Unidirectional broadband light emission from supported plasmonic nanowires", Nano letters **11**, 706–711 (2011).

[150]L. Novotny and N. Van Hulst, "Antennas for light", Nature photonics **5**, 83–90 (2011).

[151]Y. Yang, Q. Li, and M. Qiu, "Controlling the angular radiation of single emitters using dielectric patch nanoantennas", Applied Physics Letters **107**, 031109 (2015).

[152]Y. Yang, Q. Li, and M. Qiu, "Broadband nanophotonic wireless links and networks using on-chip integrated plasmonic antennas", Scientific reports **6** (2016).

[153]P. Biagioni, J.-S. Huang, and B. Hecht, "Nanoantennas for visible and infrared radiation", Reports on Progress in Physics **75**, 024402 (2012).

[154]H. Wei and H. Xu, "Nanowire-based plasmonic waveguides and devices for integrated nanophotonic circuits", Nanophotonics **1**, 155–169 (2012).

[155]X. Xiong, C.-L. Zou, X.-F. Ren, A.-P. Liu, Y.-X. Ye, F.-W. Sun, and G.-C. Guo, "Silver nanowires for photonics applications", Laser & Photonics Reviews **7**, 901–919 (2013).

[156]Y. Huang, Y. Fang, Z. Zhang, L. Zhu, and M. Sun, "Nanowire-supported plasmonic waveguide for remote excitation of surface-enhanced raman scattering", Light: Science & Applications **3**, e199 (2014).

[157]S. Luo, H. Yang, Y. Yang, D. Zhao, X. Chen, M. Qiu, and Q. Li, "Controlling wave-vector of propagating surface plasmon polaritons on single-crystalline gold nanoplates", Scientific reports **5** (2015).

[158]Q. H. Cui, Y. S. Zhao, and J. Yao, "Controlled synthesis of organic nanophotonic materials with specific structures and compositions", Advanced Materials **26**, 6852–6870 (2014).

[159]S. Mokkapati, D. Saxena, H. H. Tan, and C. Jagadish, "Optical design of nanowire absorbers for wavelength selective photodetectors", Scientific reports **5** (2015).

[160]D. Saxena, F. Wang, Q. Gao, S. Mokkapati, H. H. Tan, and C. Jagadish, "Mode profiling of semiconductor nanowire lasers", Nano letters **15**, 5342–5348 (2015).

[161]Y. Fontana, G. Grzela, E. P. Bakkers, and J. G. Rivas, "Mapping the directional emission of quasi-two-dimensional photonic crystals of semiconductor nanowires using fourier microscopy", Physical Review B **86**, 245303 (2012).

[162]J. Kjelstrup-Hansen, C. Simbrunner, and H.-G. Rubahn, "Organic surface-grown nanowires for functional devices", Reports on Progress in Physics **76**, 126502 (2013).

[163]D. Singh, A. Dasgupta, V. Aswathy, R. P. Tripathi, and G. P. Kumar, "Directional outcoupling of light from a plasmonic nanowire-nanoparticle junction", Optics letters **40**, 1006–1009 (2015).

[164]G. P. Kumar, "Plasmonic nano-architectures for surface enhanced raman scattering: a review", Journal of Nanophotonics **6**, 064503–1 (2012).

[165]Y. S. Zhao, *Organic nanophotonics: fundamentals and applications* (Springer, 2014).

[166]R. Chikkaraddy, D. Singh, and G. Pavan Kumar, "Plasmon assisted light propagation and raman scattering hot-spot in end-to-end coupled silver nanowire pairs", Applied Physics Letters **100**, 043108 (2012).

[167]Y. S. Zhao, J. Wu, and J. Huang, "Vertical organic nanowire arrays: controlled synthesis and chemical sensors", Journal of the American Chemical Society **131**, 3158–3159 (2009).

[168]Y. S. Zhao, P. Zhan, J. Kim, C. Sun, and J. Huang, "Patterned growth of vertically aligned organic nanowire waveguide arrays", ACS nano **4**, 1630–1636 (2010).

[169]K. Takazawa, J.-i. Inoue, K. Mitsuishi, and T. Takamasu, "Fraction of a millimeter propagation of exciton polaritons in photoexcited nanofibers of organic dye", Physical review letters **105**, 067401 (2010).

[170]K. Takazawa, J.-i. Inoue, K. Mitsuishi, and T. Takamasu, "Micrometer-scale photonic circuit components based on propagation of exciton polaritons in organic dye nanofibers", Advanced Materials **23**, 3659–3663 (2011).

[171]S Blumstengel, S Sadofev, C Xu, J Puls, and F Henneberger, "Converting wannier into frenkel excitons in an inorganic/organic hybrid semiconductor nanostructure", Physical review letters **97**, 237401 (2006).

[172]D. G. Lidzey, D. D. Bradley, A. Armitage, S. Walker, and M. S. Skolnick, "Photon-mediated hybridization of frenkel excitons in organic semiconductor microcavities", Science **288**, 1620–1623 (2000).

[173]C. J. Bardeen, "The structure and dynamics of molecular excitons", Annual review of physical chemistry **65**, 127–148 (2014).

[174]R. Chikkaraddy, P. P. Patra, R. P. Tripathi, A. Dasgupta, and G. P. Kumar, "Plasmon-controlled excitonic emission from vertically-tapered organic nanowires", Nanoscale **8**, 14803–14808 (2016).

[175]R. P. Tripathi, R. Chikkaraddy, A. Dasgupta, and G. Pavan Kumar, "Directional exciton-polariton photoluminescence emission from terminals of a microsphere-coupled organic waveguide", Applied Physics Letters **108**, 031102 (2016).

[176]R. P. Tripathi, A. Dasgupta, R. Chikkaraddy, P. P. Patra, A. B. Vasista, and G. P. Kumar, "Optics of an individual organic molecular mesowire waveguide: directional light emission and anomalous refractive index", Journal of Optics **18**, 065002 (2016).

[177]Y. S. Zhao, A. Peng, H. Fu, Y. Ma, and J. Yao, "Nanowire waveguides and ultraviolet lasers based on small organic molecules", Advanced Materials **20**, 1661–1665 (2008).

[178]H. Dong, Y. Wei, W. Zhang, C. Wei, C. Zhang, J. Yao, and Y. S. Zhao, "Broadband tunable microlasers based on controlled intramolecular charge-transfer process in organic supramolecular microcrystals", Journal of the American Chemical Society **138**, 1118–1121 (2016).

[179]X. Wang, Q. Liao, Z. Xu, Y. Wu, L. Wei, X. Lu, and H. Fu, "Exciton-polaritons with size-tunable coupling strengths in self-assembled organic microresonators", ACS Photonics **1**, 413–420 (2014).

[180]C. Zhang, C.-L. Zou, Y. Yan, R. Hao, F.-W. Sun, Z.-F. Han, Y. S. Zhao, and J. Yao, "Two-photon pumped lasing in single-crystal organic nanowire exciton polariton resonators", Journal of the American Chemical Society **133**, 7276–7279 (2011).

[181]R. Chandrasekar, "Organic photonics: prospective nano/micro scale passive organic optical waveguides obtained from π-conjugated ligand molecules", Physical Chemistry Chemical Physics **16**, 7173–7183 (2014).

[182]N. Chandrasekhar, M. A. Mohiddon, and R. Chandrasekar, "Organic submicro tubular optical waveguides: self-assembly, diverse geometries, efficiency, and remote sensing properties", Advanced Optical Materials **1**, 305–311 (2013).

[183]L. Novotny and B. Hecht, *Principles of nano-optics* (Cambridge university press, 2012).

[184]W Lukosz and R. Kunz, "Light emission by magnetic and electric dipoles close to a plane interface. i. total radiated power", JOSA **67**, 1607–1615 (1977).

[185]W Lukosz and R. Kunz, "Light emission by magnetic and electric dipoles close to a plane dielectric interface. ii. radiation patterns of perpendicular oriented dipoles", JOSA **67**, 1615–1619 (1977).

[186]W. Barnes, "Fluorescence near interfaces: the role of photonic mode density", journal of modern optics **45**, 661–699 (1998).

[187]P. Bhattacharya, B. Xiao, A. Das, S. Bhowmick, and J. Heo, "Solid state electrically injected exciton-polariton laser", Physical review letters **110**, 206403 (2013).

[188]A Imamog, R. Ram, S Pau, Y Yamamoto, et al., "Nonequilibrium condensates and lasers without inversion: exciton-polariton lasers", Physical Review A **53**, 4250 (1996).

[189]Y. Yan and Y. S. Zhao, "Organic nanophotonics: from controllable assembly of functional molecules to low-dimensional materials with desired photonic properties", Chemical Society Reviews **43**, 4325–4340 (2014).

[190]M. Schiek, F. Balzer, K. Al-Shamery, J. R. Brewer, A. Lützen, and H.-G. Rubahn, "Organic molecular nanotechnology", Small **4**, 176–181 (2008).

[191]F. Balzer, V. G. Bordo, A. C. Simonsen, and H.-G. Rubahn, "Optical waveguiding in individual nanometer-scale organic fibers", Physical Review B **67**, 115408 (2003).

[192]P. Simesen, T. Søndergaard, E. Skovsen, J. Fiutowski, H.-G. Rubahn, S. I. Bozhevolnyi, and K. Pedersen, "Surface plasmon polariton excitation by second harmonic generation in single organic nanofibers", Optics express **23**, 16356–16363 (2015).

[193]B. E. Saleh, M. C. Teich, and B. E. Saleh, *Fundamentals of photonics*, Vol. 22 (Wiley New York, 1991).

[194]D. Singh, M. Raghuwanshi, and G. Pavan Kumar, "Propagation of light in serially coupled plasmonic nanowire dimer: geometry dependence and polarization control", Applied Physics Letters **101**, 111111 (2012).

[195]Y. Sun, Y. Yin, B. T. Mayers, T. Herricks, and Y. Xia, "Uniform silver nanowires synthesis by reducing agno3 with ethylene glycol in the presence of seeds and poly (vinyl pyrrolidone)", Chemistry of Materials **14**, 4736–4745 (2002).

[196]T. Shegai, V. D. Miljkovic, K. Bao, H. Xu, P. Nordlander, P. Johansson, and M. Kall, "Unidirectional broadband light emission from supported plasmonic nanowires", Nano letters **11**, 706–711 (2011).

[197]J. A. Schuller, S. Karaveli, T. Schiros, K. He, S. Yang, I. Kymissis, J. Shan, and R. Zia, "Orientation of luminescent excitons in layered nanomaterials", Nature nanotechnology **8**, 271–276 (2013).

[198]J. Takahara, S. Yamagishi, H. Taki, A. Morimoto, and T. Kobayashi, "Guiding of a one-dimensional optical beam with nanometer diameter", Optics letters **22**, 475–477 (1997).

[199]X. Xiong, C.-L. Zou, X.-F. Ren, A.-P. Liu, Y.-X. Ye, F.-W. Sun, and G.-C. Guo, "Silver nanowires for photonics applications", Laser & Photonics Reviews **7**, 901–919 (2013).

[200]D. E. Chang, A. S. Sørensen, P. Hemmer, and M. Lukin, "Strong coupling of single emitters to surface plasmons", Physical Review B **76**, 035420 (2007).